International Journal of Solids and Structures 224 (2021) 111040

Contents lists available at ScienceDirect

International Journal of Solids and Structures

journal homepage: www.elsevier.com/locate/ijsolstr

# Mean field interaction model accounting for the spatial distribution of inclusions in elastic-viscoplastic composites

K. Kowalczyk-Gajewska [a,*], M. Majewski [a], S. Mercier [b], A. Molinari [b]

[a] Institute of Fundamental Technological Research, Polish Academy of Sciences, Pawińskiego 5B, 02-106 Warsaw, Poland
[b] Université de Lorraine – CNRS – Arts et Métiers ParisTech, Laboratoire d'Etude des Microstructures et de Mécanique des Matériaux, 7 rue Felix Savart, 57070 Metz, France

ARTICLE INFO

*Article history:*
Received 29 January 2021
Received in revised form 19 March 2021
Accepted 22 March 2021
Available online 27 March 2021

Dedicated to Professor Henryk Petryk on the occasion of his 70th birthday.

*Keywords:*
Homogenization
The cluster interaction model
Elastic-viscoplastic composite
Spatial configuration of inclusions
Interaction between inclusions

ABSTRACT

A cluster interaction model has been proposed to account for the spatial distribution and morphology of particles when estimating the effective properties of elastic and thermoelastic composites (Molinari and El Mouden, 1996). In the present paper this approach is extended to elastic-viscoplastic composites. To this end the tangent linearization of the non-linear viscoplastic law and the concept of additive interaction equation are used. Although the extension is formulated for the non-linear case, first applications are considered for linear viscoelastic composites, a situation rich enough to evaluate the interest of the cluster interaction approach. Results of the model are compared to numerical homogenization for periodic unit cells with two cubic configurations.

© 2021 The Author(s). Published by Elsevier Ltd. This is an open access article under the CC BY license (http://creativecommons.org/licenses/by/4.0/).

## 1. Introduction

The role of inclusion packing in a composite has been a subject of investigation in the literature since decades. Indeed, capturing the effect of the spatial distribution of inclusions on the effective properties of interest is crucial for the development of composite materials, especially today with the material by design trend. This research field concerns multiple domains of physics (heat transfer, chemical diffusion, mechanics...). For mechanics, homogenization approaches have been widely developed for characterizing the overall response and local fields (stress and strain per phase). In general, the internal structure of composite materials is characterized by the volume fraction of phases and by their morphological configuration i.e. by the shape and orientation of inclusions. We consider here the additional information provided by the topological configuration of phases, i.e. their spatial distribution. This aspect is getting a particular importance with the development of architectured materials that is allowed by modern fabrication techniques such as additive manufacturing. With these techniques it is feasible to design the internal material configuration according to a regular pattern. This pattern characterizes the topological configuration of the composite.

Early models have been proposed for evaluating the thermal conductivity and its link to the spatial distribution of inclusions. Rayleigh (1892) considered a simple cubic lattice of spheres in a homogeneous material and evaluated its conductivity. McKenzie et al., 1978; McPhedran and McKenzie, 1978; Sangani and Acrivos, 1982, derived the effective thermal conductivity of a periodic array of spheres. Lu (1999) and Mercier et al. (2000) adopted a rectangular array of spheroids. They were able to analyse the effect of the unit cell aspect ratio on the conductivity predictions.

Similarly, several contributions have analyzed the effect of inclusion arrangements on the overall mechanical response of composites. Nemat-Nasser et al. (1982) were able to derive analytical expressions for the overall elastic moduli of a composite containing periodically distributed inclusions in the elastic matrix. The derived moduli were expressed in terms of series. Sangani and Lu (1987) evaluated the elasticity tensor of a composite with spherical elastic particles. Inclusions were distributed along simple, body-centered and face-centered cubic arrays. Rodin (1993) proposed a different approach based on the eigenstrain method. Predicted elastic moduli obtained by Rodin (1993) for a regular periodic arrays of spheres were compared to finite element calculations. A good agreement was observed. A different approach was proposed in Molinari and El Mouden (1996) and named hereafter as the cluster interaction model. Elastic inclusions were embedded in an isotropic elastic medium. The approach was based on the Lippman-Schwinger-Dyson equation derived in the context of

* Corresponding author.
*E-mail address:* kkowalcz@ippt.pan.pl (K. Kowalczyk-Gajewska).

https://doi.org/10.1016/j.ijsolstr.2021.111040
0020-7683/© 2021 The Author(s). Published by Elsevier Ltd.
This is an open access article under the CC BY license (http://creativecommons.org/licenses/by/4.0/).

heterogeneous elasticity. The morphological and spatial distributions of particles were taken into account in this scheme. One of the goals was to improve the predictions of classical homogenization schemes at finite concentrations of inclusions (for instance Mori-Tanaka scheme) by taking into account the interaction between inclusions. El Mouden et al. (1998) extended the range of applications of the cluster model by considering coated inclusions. El Mouden and Molinari (2000) generalized the cluster model to the case of ellipsoidal thermoelastic inclusions embedded in an anisotropic thermoelastic matrix (under the assumption of uniform temperature in the medium). As already mentioned above, the cluster model was also adopted to derive the thermal conductivity of composite with coated inclusions in Mercier et al. (2000). The effect of the spatial distribution and of the coating thickness compared well with results of the literature (Hatta and Taya, 1986; Lu and Song, 1996). Based on the eigenstrain theory and Eshelby's equivalence principle, multiple inclusion interaction was proposed by Schjødt-Thomsen and Pyrz (2005). By considering a cubic arrangement, the predictions of the overall elastic response were shown to be highly influenced by the inclusion separation distance. Note that the packing effect, as described by a mean minimum distance of inclusions or its statistical distribution, can be accounted for also by the so-called morphologically representative pattern (MRP) approach developed by Bornert et al. (1996) and Marcadon et al. (2007) and numerically validated by Majewski et al. (2017) and Majewski et al. (2020) for elastic and elastic-plastic composites, respectively. However, this mean-field scheme is not able to account for the spatial distribution of inclusions. Ponte Castañeda and Willis (1995) developed a variational approach to account for spatial distribution of inclusions for particulate composites. The authors proposed new Hashin-Strickman type of bounds for linear elasticity where inclusion shape and spatial distribution can be chosen independently by assuming that the spatial correlations of inclusion locations, described by joint probability density functions, take particular "ellipsoidal" forms and performing ensemble averaging. Note that the proposed theory was developed assuming that the composite is statistically homogeneous. Ma et al. (2004) extended the previous approach by considering various patterns. To do so, the position of the particles in the pattern was described by an ad hoc distribution. The extension to elastic-plastic behavior was also proposed adopting a secant linearization technique.

Drugan and Willis (1996) adopted also a variational approach, employing joint probability density functions, to derive the overall behavior of composites when the applied loading is spatially-varying. By approximating the ensemble average of the strain field to its Taylor series (restricted to the third order component), it was shown that the resulting macroscopic constitutive relation involves higher order terms. When considering isotropic phase distribution, the non-local response of the material was obtained explicitly. By studying the magnitude of this additional term, authors were able to give guidelines for the selection of the minimum size of a representative volume element. The procedure was applied for random elastic composites containing aligned spheroidal heterogeneities by Monetto and Drugan (2009). The impact of residual stresses on the non-local behavior was investigated by Dal Corso and Deseri (2013) and their effect on the minimum size for the RVE was discussed. Note that conceptually related results were found also by Bigoni and Drugan (2007). Indeed, the homogenized constitutive law for a dilute two-phase standard elastic composite subject to slowly varying non-uniform load exhibits non-local terms. Quadratic displacement fields were considered. Approximate Cosserat moduli were found by comparing the elastic energies of the heterogeneous medium and of the homogenized one. In a more recent work, Bacca et al. (2013a) showed that the gap between energies can be suppressed when considering a second-gradient Mindlin and Eshel elastic material instead of a Cosserat one. The outcome of the work was the analytical definition of the non-local term. Next, Bacca et al. (2013b) demonstrated that an anisotropic non-local constitutive model may emerge from particular distributions of inclusions (for instance, rectangular lattice of spherical inclusions).

A different approach to account for spatial distribution of particles was adopted by Kushch et al. (2013). From Maxwell's concept of equivalent inhomogeneity, the effective elastic properties of particulate composites were estimated. The proposed solutions, developed in terms of series, accounted for the interactions between particles of the composite. Accurate estimates of the effective elastic moduli were found for specific geometrical arrangements like simple cubic array or random dispersion of inclusions.

The literature concentrates mostly on elasticity and thermoelasticity. Here, we address the problem of particle interactions for more complex constitutive behaviors. It was observed in the literature, see for instance (Lahellec and Suquet, 2007; Czarnota et al., 2015), that in the case of composites with elastic-viscoplastic matrix and elastic inclusions, Mori-Tanaka types of approaches were not capable of capturing accurately the overall response of the composite when the volume fraction of inclusion was large. For that precise configuration, it is worth to cite the contribution of Li and Hu (2007). They considered elastic inclusions with a linear-viscoelastic matrix. They proposed to solve the two-particle interaction problem in the Laplace domain, adopting the Kuster-Toksoz model. By considering the direct interaction between particles and introducing the probability distribution function of presence of inclusion centers in the composite, they developed an enhanced model valid for finite concentration of inclusions. They proved that the new model predicts more stiff overall response than the Mori-Tanaka approach. In addition, a strong effect of the particle distribution was detected, showing that the packing of inclusions is a key ingredient for the derivation of precise estimate.

In the present paper an extension of the cluster interaction approach to elastic-viscoplastic heterogeneous media is proposed. To this end the tangent linearization of non-linear viscoplastic law (Molinari et al., 1987) and the additive interation law (Molinari, 2002) are used. The theory can be derived for several families of inclusions, see Molinari and El Mouden (1996), but we focus here on the case of a single family of inclusions.

In the model, non-linear Maxwell type behaviors are assumed for matrix and inclusions. Applications are restricted in Section 4 to linear viscoelastic composites, a framework rich enough to evaluate the interest of the cluster approach. The specific case of elastic inclusion is also particularly addressed and it is shown that the predictions of the cluster model are clearly more accurate than the classical Mori-Tanaka scheme when compared to finite element simulations. The effect of spatial distribution of inclusions is also illustrated by investigating the case of simple cubic (denoted regular cubic in the following) and body centered cubic arrays of inclusions.

## 2. The interaction cluster model for a thermoelastic medium: case of a single family of ellipsoidal heterogeneities

Molinari and El Mouden (1996) and El Mouden and Molinari (2000) proposed a mean field interaction model (also denoted in brief "cluster model") for linear elastic and thermoelastic composites. The cluster model was aimed to describe interaction effects between heterogeneities. Heterogeneities of ellipsoidal shape (also denoted as inclusions) are embedded in a uniform matrix. Each individual inclusion has uniform properties. A representative volume element (RVE) with a population of inclusions characterizing the internal structure of the composite material is considered. The RVE is reproduced by periodicity in order to fill the whole space.

From this RVE a set of $N$ families of equivalent inclusions are defined. In a given family, the inclusions are regularly disposed along a periodic array, belong to the same phase, and have same shape, same size and same orientations of principal axes. Consequently, all inclusions of a given family have same mean deformation. Then, the problem reduces to finding the solution of a system of $N$ linear equations providing the mean deformations of the representative inclusions. In that way, simple to very complex internal configurations can be analyzed by increasing the number of families from $N = 1$ to larger values. Complex particulate composites can involve several phases, various inclusion shapes and orientations or some irregularities in the spatial distribution of inclusions. An important outcome of this approach is that interactions between inclusions are described by considering their spatial distribution. The approach developed by Ma et al. (2004) bears some similarity with the mean field interaction model of Molinari and El Mouden (1996), since interactions between inclusions are described in the same way. However, the configuration analyzed by Ma et al. (2004) is restricted to clusters of inclusions (packing of inclusions), while any spatial configuration can be handled by the approach of Molinari and El Mouden (1996), from disordered to very ordered internal structures (architectured materials).

The purpose of the present paper is to extend the elastic mean field interaction model of Molinari and El Mouden (1996) to elastic-viscoplastic composites. The new difficulty is related to the higher level of complexity of the material response (see the literature review of the introduction), and therefore it is enough to restrict the presentation to a simple internal structure. Here, a single family of inclusions is considered. For an arbitrary number of families, we refer to Molinari and El Mouden (1996) and El Mouden and Molinari (2000).

### 2.1. Basic equations of the thermoelastic interaction cluster model for a single family of inclusions

We recall here basic equations of the thermoelastic interaction cluster model that are needed later. A two-phase material is considered. Phase $I$ is made up of a family of equivalent ellipsoidal inclusions, as defined above, embedded in the matrix phase $m$. The volume fraction of inclusions (phase $I$) is denoted by $f$. Each phase is governed by the following thermoelastic law:[1]

$$\boldsymbol{\sigma} = \mathbf{C}_k \cdot \boldsymbol{\epsilon} + \boldsymbol{\beta}_k \theta \tag{1}$$

with $k = I$ for inclusions and $k = m$ for matrix. $\boldsymbol{\sigma}$ is the Cauchy stress, $\boldsymbol{\epsilon}$ the strain, $\mathbf{C}_k$ the fourth order tensor of elastic moduli, $\boldsymbol{\beta}_k\theta$ the thermal stress, $\theta$ a temperature variation with respect to a reference value; $\theta$ is taken as uniform.

Denoting by $\boldsymbol{\sigma}_I$ and $\boldsymbol{\epsilon}_I$, respectively, the stress and strain averages within an inclusion, we obtain from Eq. (1):

$$\boldsymbol{\sigma}_I = \mathbf{C}_I \cdot \boldsymbol{\epsilon}_I + \boldsymbol{\beta}_I \theta \tag{2}$$

By definition, all inclusions play an equivalent role in a given family; therefore $\boldsymbol{\sigma}_I$ and $\boldsymbol{\epsilon}_I$ are the same for all inclusions.

Similarly, for the matrix phase we have:

$$\boldsymbol{\sigma}_m = \mathbf{C}_m \cdot \boldsymbol{\epsilon}_m + \boldsymbol{\beta}_m \theta \tag{3}$$

where $\boldsymbol{\sigma}_m$ and $\boldsymbol{\epsilon}_m$ are respectively stress and strain averages.

The whole space $R^3$ is filled by the composite material, and we denote by $\boldsymbol{\Sigma}$ and $\mathbf{E}$ respectively the macroscopic strain and stress. We take for homogeneous reference medium the unbounded space having the matrix thermoelastic properties. By using the Green function technique, the solution of the boundary value problem is obtained in the form of an LSD integral equation (Lipman-Schwinger-Dyson equation), see Zeller and Dederichs (1973). Then, an approximate solution for $\boldsymbol{\epsilon}_I$ is derived, see El Mouden and Molinari (2000):

$$\boldsymbol{\epsilon}_I = \boldsymbol{\epsilon}_0 - \mathbf{P}^I_* \cdot (\Delta\mathbf{C}_I \cdot \boldsymbol{\epsilon}_I + \Delta\boldsymbol{\beta}_I \theta) \tag{4}$$

with

$$\Delta\mathbf{C}_I = \mathbf{C}_I - \mathbf{C}_m, \tag{5}$$

$$\Delta\boldsymbol{\beta}_I = \boldsymbol{\beta}_I - \boldsymbol{\beta}_m, \tag{6}$$

$$\mathbf{P}^I_* = -\boldsymbol{\Gamma}^{II} - \sum_{J \neq I} \boldsymbol{\Gamma}^{IJ} = -\sum_J \boldsymbol{\Gamma}^{IJ} \tag{7}$$

The symbol $\sum_{J\neq I}$ in Eq. (7) has the following meaning. Let us attribute the label $I$ to a given inclusion. $\sum_{J\neq I}$ represents the summation made by considering all other inclusions of the family (an infinite number theoretically). Since all inclusions are playing the same role, $\mathbf{P}^I_*$ is independent of the arbitrary choice of the inclusion $I$.

The fourth order tensors $\boldsymbol{\Gamma}^{IJ}$ are defined by:

$$\boldsymbol{\Gamma}^{IJ} = \frac{1}{V_I} \int_{V_I} \int_{V_J} \boldsymbol{\Gamma}(\mathbf{r} - \mathbf{r}') d\mathbf{r}' d\mathbf{r} \tag{8}$$

where integrations are performed on the domains $V_I$ and $V_J$ occupied by inclusions $I$ and $J$ respectively. $\boldsymbol{\Gamma}^{IJ}$ depends on the shape of inclusions and the relative distance between inclusion centers; $\boldsymbol{\Gamma}^{IJ}$ is invariant under homothetic transformations of the configuration. $\boldsymbol{\Gamma}^{IJ}$ is also function of $\mathbf{C}_m$ through the kernel $\boldsymbol{\Gamma}$ in Eq. (8) which is obtained from Green functions related to the elastic stiffness $\mathbf{C}_m$ of the reference medium. For two spherical inclusions embedded in an isotropic elastic medium, $\boldsymbol{\Gamma}^{IJ}$ can be analytically expressed, Berveiller et al. (1987), see also Appendix A in Molinari and El Mouden (1996).

The evaluation of $\mathbf{P}^I_*$ involves an infinite series $\sum_J \boldsymbol{\Gamma}^{IJ}$. In practice, $\mathbf{P}^I_*$ is calculated by taking a finite number of terms in this series. Thus, we consider a sphere of radius $R_c$ whose center coincides with the one of inclusion $I$. The cluster $C(R_c)$ is constituted by the ensemble of inclusions whose center belongs to this sphere. We define:

$$\mathbf{P}^I_*(R_c) = -\sum_{J \in C(R_c)} \boldsymbol{\Gamma}^{IJ} \tag{9}$$

In applications, except otherwise specified, the cluster radius is taken large enough in order to practically achieve the convergence of the series $\sum_J \boldsymbol{\Gamma}^{IJ}$. The convergence when $R_c \to \infty$ is demonstrated in Molinari and El Mouden (1996), Appendix B. The case of a cluster of zero radius containing the single inclusion $I$ will be also analyzed later in Section 2.2.

In Eq. (4), $\boldsymbol{\epsilon}_0$ is an integration constant that appears in the LSD integral equation. By taking the volume average of the LSD integral equation it was shown by El Mouden and Molinari (2000) that:

$$\boldsymbol{\epsilon}_0 = \mathbf{E} + \mathbf{P}^0 \cdot \langle \Delta\mathbf{C} \cdot \boldsymbol{\epsilon} + \Delta\boldsymbol{\beta}\theta \rangle, \tag{10}$$

where $\langle . \rangle$ designates volume average, $\Delta\mathbf{C} = \Delta\mathbf{C}_I, \Delta\boldsymbol{\beta} = \Delta\boldsymbol{\beta}_I$ in inclusions, see Eqs. (5,6), and $\Delta\mathbf{C} = \mathbf{0}, \Delta\boldsymbol{\beta} = \mathbf{0}$ in the matrix. Consequently, Eq. (10) can be written as:

$$\boldsymbol{\epsilon}_0 = \mathbf{E} + f\mathbf{P}^0 \cdot (\Delta\mathbf{C}_I \cdot \boldsymbol{\epsilon}_I + \Delta\boldsymbol{\beta}_I \theta). \tag{11}$$

The polarization tensor $\mathbf{P}^0$ is defined by:

$$\mathbf{P}^0(\mathbf{C}_m) = -\boldsymbol{\Gamma}^{II}(\text{sphere}) \tag{12}$$

where $\boldsymbol{\Gamma}^{II}(\text{sphere})$ is calculated with Eq. (8) (with $I = J$) for an inclusion of spherical shape and by using the tensor of elastic moduli $\mathbf{C}_m$ of the reference medium. Therefore, $\mathbf{P}^0$ is solely function of $\mathbf{C}_m$.

[1] Notation: $\cdot$ is a full contraction of the second order tensor with a fourth order tensor, while $\circ$, appearing e.g. in Eq. (28), is a double contraction of two fourth order tensors.

The strains $\boldsymbol{\epsilon}_I, \boldsymbol{\epsilon}_m$ and $\boldsymbol{\epsilon}_0$ are obtained in terms of $\mathbf{E}$ and $\theta$ by solving the linear set of Eqs. (4), (11) and (13) below:

$$\mathbf{E} = f\boldsymbol{\epsilon}_I + (1-f)\boldsymbol{\epsilon}_m \tag{13}$$

Eq. (4) and Eq. (11) are now written in a form useful for addressing the elastic-viscoplastic problem. We define the stress $\boldsymbol{\sigma}_0$ as being related to $\boldsymbol{\epsilon}_0$ by the constitutive response of the matrix, Eq. (3):

$$\boldsymbol{\sigma}_0 = \mathbf{C}_m \cdot \boldsymbol{\epsilon}_0 + \boldsymbol{\beta}_m \theta \tag{14}$$

Substracting Eq. (14) from the inclusion's constitutive law, Eq. (2), we obtain:

$$\boldsymbol{\sigma}_I - \boldsymbol{\sigma}_0 = \mathbf{C}_I \cdot \boldsymbol{\epsilon}_I - \mathbf{C}_m \cdot \boldsymbol{\epsilon}_0 + \Delta\boldsymbol{\beta}_I \theta \tag{15}$$

Using this relationship to eliminate $\Delta\boldsymbol{\beta}_I\theta$ in Eq. (4), we end up with the following interaction law and its inverted form:

$$\boldsymbol{\sigma}_I - \boldsymbol{\sigma}_0 = -\mathbf{C}_*^I \cdot (\boldsymbol{\epsilon}_I - \boldsymbol{\epsilon}_0) \tag{16}$$

$$\boldsymbol{\epsilon}_I - \boldsymbol{\epsilon}_0 = -\mathbf{M}_*^I \cdot (\boldsymbol{\sigma}_I - \boldsymbol{\sigma}_0) \tag{17}$$

with

$$\mathbf{C}_*^I = \left(\mathbf{P}_*^I\right)^{-1} - \mathbf{C}_m \tag{18}$$

$$\mathbf{M}_*^I = \left(\mathbf{C}_*^I\right)^{-1} \tag{19}$$

It can be noted that $\mathbf{P}_*^I$ and $\mathbf{C}_*^I$ play similar roles as respectively the polarization tensor and the Hill tensor in the classical elastic mean field scheme based on the Eshelby solution of the ellipsoidal heterogeneity problem, Hill (1965).

Another result that is used in the following is obtained by transforming Eq. (11) into (see Appendix A):

$$\mathbf{E} - \boldsymbol{\epsilon}_0 = -\mathbf{M}_*^0 \cdot (\boldsymbol{\Sigma} - \boldsymbol{\sigma}_0) \tag{20}$$

with

$$\mathbf{M}_*^0 = \left(\left(\mathbf{P}^0\right)^{-1} - \mathbf{C}_m\right)^{-1} \tag{21}$$

### 2.2. Comparison with the Mori-Tanaka model

It is shown here that the cluster model with $R_c = 0$ (vanishing cluster radius) coincides with the Mori-Tanaka model when inclusions are spherical.

For $R_c = 0$ , and with $\mathbf{P}^0$ defined by Eq. (12), we can write Eq. (7) as:

$$\mathbf{P}_*^I = -\boldsymbol{\Gamma}^{II}(\text{sphere}) = \mathbf{P}^0 \tag{22}$$

Then, Eq. (4) reads:

$$\boldsymbol{\epsilon}_I = \boldsymbol{\epsilon}_0 - \mathbf{P}^0 \cdot (\Delta\mathbf{C}_I \cdot \boldsymbol{\epsilon}_I + \Delta\boldsymbol{\beta}_I\theta). \tag{23}$$

By elimination of $\mathbf{P}^0 \cdot (\Delta\mathbf{C}_I \cdot \boldsymbol{\epsilon}_I + \Delta\boldsymbol{\beta}_I\theta)$ between Eq. (11) and Eq. (23) we get $(1-f)\boldsymbol{\epsilon}_0 = \mathbf{E} - f\boldsymbol{\epsilon}_I$. Then, Eq. (13) leads to:

$$\boldsymbol{\epsilon}_0 = \boldsymbol{\epsilon}_m \tag{24}$$

Eq. (23) provides the following localization law for the strain within inclusions:

$$\boldsymbol{\epsilon}_I = \left(\mathbf{I} + \mathbf{P}^0 \cdot \Delta\mathbf{C}_I\right)^{-1} \cdot \left(\boldsymbol{\epsilon}_m - \mathbf{P}^0 \cdot \Delta\boldsymbol{\beta}_I\theta\right). \tag{25}$$

The strains $\boldsymbol{\epsilon}_I$ and $\boldsymbol{\epsilon}_m$ are given in terms of the macroscopic applied strain $\mathbf{E}$ by Eq. (13) and (25). These strains are identical to those derived from the Mori-Tanaka model.

### 2.3. Investigating interaction effects between inclusions through different homogenization models

In the Mori-Tanaka model interactions between inclusions are solely represented by their volume fraction $f$. In the cluster model interaction effects are accounted for at a higher level through $f$ and the following interaction tensor:

$$\mathbf{P}_{\text{int}}^{*I} = -\sum_{J \neq I} \boldsymbol{\Gamma}^{IJ} \tag{26}$$

This tensor appears in the definition (7) of $\mathbf{P}_*^I$:

$$\mathbf{P}_*^I = -\boldsymbol{\Gamma}^{II} + \mathbf{P}_{\text{int}}^{*I} \tag{27}$$

For the purpose of investigating interaction effects, we define another model (for spherical inclusions), denoted henceforth as hybrid model, based on the same equations as the cluster model except for the definition of $\boldsymbol{\epsilon}_0$, Eq. (11), which is replaced by Eq. (24) of the Mori-Tanaka model. In the following we shall denote by CM1 the original cluster model and by CM2 the hybrid version. The interest of model CM2 comes from the way interaction effects are appearing in the localization law providing the strain in inclusions in terms of $\mathbf{E}$ and $\theta$:

$$\boldsymbol{\epsilon}_I = \left[\mathbf{I} + \left((1-f)\mathbf{P}^0 + (1-f)\mathbf{P}_{\text{int}}^{*I}\right) \circ \Delta\mathbf{C}_I\right]^{-1} \cdot \left(\mathbf{E} - \left((1-f)\mathbf{P}^0 + (1-f)\mathbf{P}_{\text{int}}^{*I}\right) \cdot \Delta\boldsymbol{\beta}_I\theta\right) \tag{28}$$

This results is obtained for spherical inclusions, by combining Eq. (4) of the cluster model with the condition $\boldsymbol{\epsilon}_0 = \boldsymbol{\epsilon}_m$ to obtain $\boldsymbol{\epsilon}_I = \boldsymbol{\epsilon}_m - \mathbf{P}_*^I.(\Delta\mathbf{C}_I \cdot \boldsymbol{\epsilon}_I + \Delta\boldsymbol{\beta}_I\theta)$. Eliminating $\boldsymbol{\epsilon}_m$ with Eq. (13), we obtain Eq. (28) for CM2.

For the cluster model CM1 we get with Eq. (4) and Eq. (11) the following localization law:

$$\boldsymbol{\epsilon}_I = \left[\mathbf{I} + \left((1-f)\mathbf{P}^0 + \mathbf{P}_{\text{int}}^{*I}\right) \circ \Delta\mathbf{C}_I\right]^{-1} \cdot \left(\mathbf{E} - \left((1-f)\mathbf{P}^0 + \mathbf{P}_{\text{int}}^{*I}\right) \cdot \Delta\boldsymbol{\beta}_I\theta\right) \tag{29}$$

For the Mori-Tanaka model (MT) the localization law for spherical inclusions reads:

$$\boldsymbol{\epsilon}_I = \left[\mathbf{I} + (1-f)\mathbf{P}^0 \circ \Delta\mathbf{C}_I\right]^{-1} \cdot \left(\mathbf{E} - (1-f)\mathbf{P}^0 \cdot \Delta\boldsymbol{\beta}_I\theta\right) \tag{30}$$

From the examination of these equations the following hierarchy between the models can be noticed, from higher to lower interaction effects: CM1 → CM2 → MT according to the corresponding weight of $\mathbf{P}_{\text{int}}^{*I}$ in the localization laws $\mathbf{P}_{\text{int}}^{*I} \to (1-f)\mathbf{P}_{\text{int}}^{*I} \to 0$.

Differences between CM1, CM2 and MT models and predictive capabilities are now assessed with respect to numerical simulation results. In FE analyses a unit cell of prescribed arrangement of inclusions subject to the micro-periodic boundary conditions is considered as described in Majewski et al. (2017). In Fig. 1 predictions of CM1, CM2 and MT models are compared with FE simulations for the purely elastic problem ($\theta = 0$). Inclusions are assumed to be spherical with same radius. They are distributed in a regular cubic configuration. The ratio between Young's moduli of inclusion and the matrix is 10 (hard inclusions case) or 0.1 (soft inclusion case), Poisson's ratio equal to 0.3 is assumed for both phases. Note that for this configuration we have just a single family of equivalent inclusions. The effective elasticity tensor of this composite is of cubic symmetry. For such symmetry we have three elastic constants: the bulk modulus $\overline{K} = \left(\overline{C}_{1111} + 2\overline{C}_{1122}\right)/3$ and two shear moduli: $\bar{\mu}_1 = \left(\overline{C}_{1111} - \overline{C}_{1122}\right)/2, \bar{\mu}_2 = \overline{C}_{1212}$.

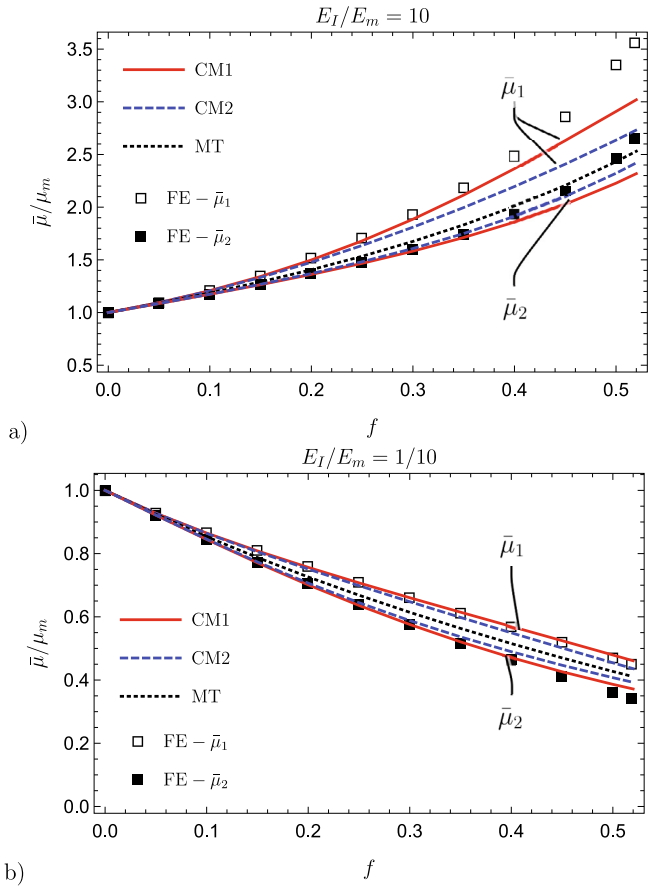


**Fig. 1.** Effective shear moduli (elastic constants) $\bar{\mu}_1 = \left(\bar{C}_{1111} - \bar{C}_{1122}\right)/2$ and $\bar{\mu}_2 = \bar{C}_{1212}$ for a two-phase composite of regular cubic distribution of inclusions. Comparison of cluster models CM1 and CM2 with FE calculations. As a reference results for the classical MT model are shown for which $\bar{\mu}_1 = \bar{\mu}_2$; a) hard inclusions: Young's moduli $E_I/E_m = 10$, b) soft inclusions: $E_I/E_m = 1/10$; Poisson's ratio $\nu_I = \nu_m = 0.3$ for both cases.

In Fig. 1 the variation of the two shear moduli with volume fraction is presented as predicted by cluster models CM1 and CM2 and FE analysis. For CM1 and CM2 models the cluster size $R_c$ is equal to $8d$ where $d$ is a minimum distance between the inclusion centers in a unit cell. It has been checked that convergence of the results is reached for this sufficiently large cluster size and any configurations adopted in the present paper. Note that for $f = 0.52$, inclusions in the regular cubic arrangement are in contact, so this is the limit volume fraction we can consider for this configuration. It is seen that for the case of stiff inclusions, results of numerical simulations are in better agreement with the original cluster model CM1 as compared to the hybrid model CM2. Very good accordance is obtained up to 0.25 volume fraction. With an increasing volume fraction the cluster model underestimates the composite stiffness.

For the soft inclusion case, both CM1 and CM2 models predict well the overall shear moduli for the whole range of volume fraction, with slightly better results for CM1 than for CM2, when compared to FE results. It should be noted that, as concerns the bulk modulus $\bar{K}$ the same value is predicted by CM1, CM2 and MT models.

The accuracy of results appears to be related to the level of interaction effects carried by models, from higher level (CM1), intermediate level (CM2) and lower level (MT), as previously described. Clearly a higher anisotropy degree of elastic stiffness, measured by the ratio $\bar{\mu}_1/\bar{\mu}_2$, is obtained for CM1 than for CM2 model. Obviously elastic stiffness is isotropic for MT model.

## 3. Elastic-viscoplastic composite

The same configuration of the composite material is considered as before, except for the constitutive behavior. Each phase is now governed by an elastic-viscoplastic law of the Maxwell-type. For phase $I$ we have:

$$\mathbf{d} = \mathbf{d}_e + \mathbf{d}_v = \mathbf{M}_I \cdot \dot{\boldsymbol{\sigma}} + \mathbf{F}_I(\mathbf{s}) \tag{31}$$

The strain rate $\mathbf{d}$ is the sum of elastic and viscoplastic parts, respectively $\mathbf{d}_e$ and $\mathbf{d}_v$. The fourth order tensor of elastic compliance is designated by $\mathbf{M}_I$. In general $\mathbf{d}_v$ is a nonlinear function of $\mathbf{s}$, the deviator of the Cauchy stress $\boldsymbol{\sigma}$.

Similarly, for the matrix phase we have:

$$\mathbf{d} = \mathbf{M}_m \cdot \dot{\boldsymbol{\sigma}} + \mathbf{F}_m(\mathbf{s}) \tag{32}$$

We successively consider the purely viscoplastic and purely elastic problems before addressing the elastic-viscoplastic case.

### 3.1. Viscoplastic case

We first consider the case of a viscoplastic response ($\mathbf{M}_I = \mathbf{0}, \mathbf{M}_m = \mathbf{0}$). Adopting the tangent linearization proposed by Molinari et al. (1987), the nonlinear response of phase $k$, $\mathbf{d}_v = \mathbf{F}_k(\mathbf{s})$ ($k = I$ for inclusions, $k = m$ for matrix) is approximated by:

$$\mathbf{d}_v = \mathbf{M}_k^{tg}(\mathbf{s}_k) \cdot \mathbf{s} + \mathbf{d}_k^{ref}(\mathbf{s}_k) \tag{33}$$

where $\mathbf{s}_k$ is the mean deviatoric stress in phase $k$, and:

$$\mathbf{M}_k^{tg}(\mathbf{s}_k) = \frac{\partial \mathbf{F}_k}{\partial \mathbf{s}}(\mathbf{s}_k) \tag{34}$$

$$\mathbf{d}_k^{ref}(\mathbf{s}_k) = \mathbf{F}_k(\mathbf{s}_k) - \mathbf{M}_k^{tg}(\mathbf{s}_k) \cdot \mathbf{s}_k \tag{35}$$

The mean strain rate associated to $\mathbf{s}_k$ is given by:

$$\mathbf{d}_v^k = \mathbf{F}_k(\mathbf{s}_k) = \mathbf{M}_k^{tg}(\mathbf{s}_k) \cdot \mathbf{s}_k + \mathbf{d}_k^{ref}(\mathbf{s}_k) \tag{36}$$

We note that the second equality in Eq. (36) results from the fact that the tangent law coincides at $\mathbf{s}_k$ with the nonlinear response $\mathbf{F}_k(\mathbf{s}_k)$ as indicated by Eq. (35).

The relationship (33) can be inverted into:

$$\mathbf{s} = \mathbf{C}_k^{tg}(\mathbf{s}_k) \cdot \mathbf{d}_v + \mathbf{s}_k^{ref}(\mathbf{s}_k) \tag{37}$$

with

$$\mathbf{s}_k^{ref} = -\mathbf{C}_k^{tg} \cdot \mathbf{d}_k^{ref} \tag{38}$$

The viscoplastic stiffness is defined by:

$$\mathbf{C}_k^{tg} = \left(\mathbf{M}_k^{tg}\right)^{-1} \tag{39}$$

Eq. (37) is formally equivalent to the thermoelastic Duhamel law, Eq. (1), with $\mathbf{d}_v$ and $\mathbf{s}_k^{ref}$ playing respectively the role of strain and thermal stress.

Taking as a reference medium the homogeneous material with constitutive response given by the matrix tangent law (Eq. (37) with $k = m$), we obtain from the thermoelastic results of Section 2.1 (Eq. (4) with $\boldsymbol{\epsilon}_I \to \mathbf{d}_v^I, \Delta\boldsymbol{\beta}_I\theta \to \Delta\mathbf{s}_I^{ref}, \mathbf{P}_*^I \to \mathbf{P}_{*v}^I$):

$$\mathbf{d}_v^I = \mathbf{d}_v^0 - \mathbf{P}_{*v}^I \cdot \left(\Delta\mathbf{C}_I^{tg} \cdot \mathbf{d}_v^I + \Delta\mathbf{s}_I^{ref}\right) \tag{40}$$

with

$$\Delta\mathbf{C}_I^{tg} = \mathbf{C}_I^{tg} - \mathbf{C}_m^{tg}, \tag{41}$$

$$\Delta\mathbf{s}_I^{ref} = \mathbf{s}_I^{ref} - \mathbf{s}_m^{ref}, \tag{42}$$

We have also introduced the following polarisation tensor:

$$\mathbf{P}^{I}_{*\mathrm{v}}(\mathbf{C}^{\mathrm{tg}}_{m}) = -\sum_{J}\boldsymbol{\Gamma}^{IJ}_{\mathrm{v}} \tag{43}$$

The tensors $\boldsymbol{\Gamma}^{IJ}_{\mathrm{v}}$ $(J = 1, 2, \ldots)$ are defined by Eq. (8) with $\boldsymbol{\Gamma}$ obtained from the Green functions depending upon the tangent modulus $\mathbf{C}^{\mathrm{tg}}_{m}$ of the reference medium.

In this interaction model, $\mathbf{d}^{0}_{\mathrm{v}}$ is an integration constant appearing in the LSD integral equation. As for the relationship (11) of the thermoelastic cluster model we have (with $\boldsymbol{\epsilon}_0 \rightarrow \mathbf{d}^{0}_{\mathrm{v}}$ and $\mathbf{E} \rightarrow \mathbf{D}_{\mathrm{v}}$):

$$\mathbf{d}^{0}_{\mathrm{v}} = \mathbf{D}_{\mathrm{v}} + f\mathbf{P}^{0}_{\mathrm{v}} \cdot \left(\Delta\mathbf{C}^{\mathrm{tg}}_{I} \cdot \mathbf{d}^{I}_{\mathrm{v}} + \Delta\mathbf{s}^{\mathrm{ref}}_{I}\right) \tag{44}$$

where $\mathbf{D}_{\mathrm{v}}$ is the macroscopic applied strain rate, and

$$\mathbf{P}^{0}_{\mathrm{v}} = -\boldsymbol{\Gamma}^{II}_{\mathrm{v}}(\mathrm{sphere}) \tag{45}$$

$\boldsymbol{\Gamma}^{II}_{\mathrm{v}}(\mathrm{sphere})$ is calculated with Eq. (8) for an inclusion of spherical shape and with the tangent modulus $\mathbf{C}^{\mathrm{tg}}_{m}$ of the reference medium. Thus, $\mathbf{P}^{0}_{\mathrm{v}}$ is solely function of $\mathbf{C}^{\mathrm{tg}}_{m}$.

We define the deviatoric stress $\mathbf{s}_0$ as being related to $\mathbf{d}^{0}_{\mathrm{v}}$ by the tangent law of the reference medium (Eq. (37) with $k = m$):

$$\mathbf{s}_0 = \mathbf{C}^{\mathrm{tg}}_{m}(\mathbf{s}_m) \cdot \mathbf{d}^{0}_{\mathrm{v}} + \mathbf{s}^{\mathrm{ref}}_{m}(\mathbf{s}_m) \tag{46}$$

Substracting Eq. (46) from the inclusion's tangent law (Eq. (37) with $k = I$) we obtain:

$$\mathbf{s}_I - \mathbf{s}_0 = \mathbf{C}^{\mathrm{tg}}_{I} \cdot \mathbf{d}^{I}_{\mathrm{v}} - \mathbf{C}^{\mathrm{tg}}_{m} \cdot \mathbf{d}^{0}_{\mathrm{v}} + \Delta\mathbf{s}^{\mathrm{ref}}_{I} \tag{47}$$

Using this relationship to eliminate $\Delta\mathbf{s}^{\mathrm{ref}}_{I}$ in Eq. (40), leads to the following interaction laws:

$$\left(\mathbf{C}^{\mathrm{tg}}_{m} - \left(\mathbf{P}^{I}_{*\mathrm{v}}\right)^{-1}\right) \cdot \left(\mathbf{d}^{I}_{\mathrm{v}} - \mathbf{d}^{0}_{\mathrm{v}}\right) = \mathbf{s}_I - \mathbf{s}_0 \tag{48}$$

or

$$\mathbf{d}^{I}_{\mathrm{v}} - \mathbf{d}^{0}_{\mathrm{v}} = \left(\mathbf{C}^{\mathrm{tg}}_{m} - \left(\mathbf{P}^{I}_{*\mathrm{v}}\right)^{-1}\right)^{-1} \cdot (\mathbf{s}_I - \mathbf{s}_0) \tag{49}$$

The definition (44) of $\mathbf{d}^{0}_{\mathrm{v}}$ given by the cluster model can be written as

$$\mathbf{D}_{\mathrm{v}} - \mathbf{d}^{0}_{\mathrm{v}} = \left(\mathbf{C}^{\mathrm{tg}}_{m} - \left(\mathbf{P}^{0}_{\mathrm{v}}\right)^{-1}\right)^{-1} \cdot (\mathbf{S} - \mathbf{s}_0) \tag{50}$$

where $\mathbf{S}$ is the deviator of the macroscopic stress $\boldsymbol{\Sigma}$. The derivation of Eq. (50) follows the same lines as for Eq. (20) in the thermoelastic case, see Appendix A.

Eqs. (49,50) can be written as:

$$\mathbf{d}^{I}_{\mathrm{v}} - \mathbf{d}^{0}_{\mathrm{v}} = -\mathbf{M}^{I}_{*\mathrm{v}} \cdot (\mathbf{s}_I - \mathbf{s}_0) \tag{51}$$

$$\mathbf{D}_{\mathrm{v}} - \mathbf{d}^{0}_{\mathrm{v}} = -\mathbf{M}^{0}_{*\mathrm{v}} \cdot (\mathbf{s}_I - \mathbf{s}_0) \tag{52}$$

with

$$\mathbf{M}^{I}_{*\mathrm{v}} = \left(\left(\mathbf{P}^{I}_{*\mathrm{v}}\right)^{-1} - \mathbf{C}^{\mathrm{tg}}_{m}\right)^{-1} \tag{53}$$

$$\mathbf{M}^{0}_{*\mathrm{v}} = \left(\left(\mathbf{P}^{0}_{\mathrm{v}}\right)^{-1} - \mathbf{C}^{\mathrm{tg}}_{m}\right)^{-1} \tag{54}$$

### 3.2. Elastic case

A linear elastic response is now assumed. Thus, the results of this section can be directly obtained by setting $\theta = 0$ in the equations of the thermoelastic case, Section 2. We express here the problem in rate form, having in view applications in elasto-viscoplasticity. For the sake of notations, and for a better understanding of how the elastic-viscoplastic interaction cluster model is built, it is convenient to explicit the equations of the elastic problem.

For each phase the rate form of the Hooke's law reads ($k = I$ for inclusions, $k = m$ for matrix):

$$\dot{\boldsymbol{\sigma}}_k = \mathbf{C}_k \cdot \mathbf{d}^{k}_{\mathrm{e}} \tag{55}$$

where $\mathbf{C}_k, \dot{\boldsymbol{\sigma}}_k$ and $\mathbf{d}^{k}_{\mathrm{e}}$ are respectively the tensor of elastic moduli, the stress rate and elastic strain rate in phase $k$. Here, we consider small deformations and "dot" represents the material derivative. For large deformations, an objective derivative (for instance Jaumann) should be used. Averages of stress and strain rate per phases are considered.

Relationships similar to Eq. (14), with $\theta = 0$, and to Eq. (17) and Eq. (20) are obtained in rate form:

- definition of $\dot{\boldsymbol{\sigma}}_0$,

$$\dot{\boldsymbol{\sigma}}_0 = \mathbf{C}_m \cdot \mathbf{d}^{0}_{\mathrm{e}} \tag{56}$$

- interaction law,

$$\mathbf{d}^{I}_{\mathrm{e}} - \mathbf{d}^{0}_{\mathrm{e}} = \left(\mathbf{C}_m - \left(\mathbf{P}^{I}_{*\mathrm{e}}\right)^{-1}\right)^{-1} \cdot (\dot{\boldsymbol{\sigma}}_I - \dot{\boldsymbol{\sigma}}_0) \tag{57}$$

- and relationship resulting from the definition of the integration constant $\mathbf{d}^{0}_{\mathrm{e}}$,

$$\mathbf{D}_{\mathrm{e}} - \mathbf{d}^{0}_{\mathrm{e}} = \left(\mathbf{C}_m - \left(\mathbf{P}^{0}_{\mathrm{e}}\right)^{-1}\right)^{-1} \cdot (\dot{\boldsymbol{\Sigma}} - \dot{\boldsymbol{\sigma}}_0) \tag{58}$$

As for Eq. (43) and Eq. (45) (or Eq. (9) and Eq. (12)) we have:

$$\mathbf{P}^{I}_{*\mathrm{e}} = -\sum_{J}\boldsymbol{\Gamma}^{IJ}_{\mathrm{e}} \tag{59}$$

$$\mathbf{P}^{0}_{\mathrm{e}} = -\boldsymbol{\Gamma}^{II}_{\mathrm{e}}(\mathrm{sphere}) \tag{60}$$

Tensors $\boldsymbol{\Gamma}^{II}_{\mathrm{e}}(\mathrm{sphere})$ and $\boldsymbol{\Gamma}^{IJ}_{\mathrm{e}}$ $(J = 1, 2, \ldots)$ are defined by Eq. (8) with $\boldsymbol{\Gamma}$ obtained from the Green functions associated to the elastic modulus $\mathbf{C}_m$ of the reference medium (matrix response). $\boldsymbol{\Gamma}^{II}_{\mathrm{e}}(\mathrm{sphere})$ is calculated for a spherical shape and consequently is solely function of $\mathbf{C}_m$.

The integration constant, $\mathbf{d}^{0}_{\mathrm{e}}$, in the elastic cluster model is given by:

$$\mathbf{d}^{0}_{\mathrm{e}} = \mathbf{D}_{\mathrm{e}} + f\mathbf{P}^{0}_{\mathrm{e}} \cdot \left(\Delta\mathbf{C}_I \cdot \mathbf{d}^{I}_{\mathrm{e}}\right) \tag{61}$$

Eq. (58) is obtained from Eq. (61) as Eq. (50) was derived from Eq. (44) in the viscoplastic cluster model (or as Eq. (20) resulted from Eq. (11) in the thermoelastic case of Section 2).

Eqs. (57,58) can be written as:

$$\mathbf{d}^{I}_{\mathrm{e}} - \mathbf{d}^{0}_{\mathrm{e}} = -\mathbf{M}^{I}_{*\mathrm{e}} \cdot (\dot{\boldsymbol{\sigma}}_I - \dot{\boldsymbol{\sigma}}_0) \tag{62}$$

$$\mathbf{D}_{\mathrm{e}} - \mathbf{d}^{0}_{\mathrm{e}} = -\mathbf{M}^{0}_{*\mathrm{e}} \cdot (\dot{\boldsymbol{\Sigma}} - \dot{\boldsymbol{\sigma}}_0) \tag{63}$$

with

$$\mathbf{M}^{I}_{*\mathrm{e}} = \left(\left(\mathbf{P}^{I}_{*\mathrm{e}}\right)^{-1} - \mathbf{C}_m\right)^{-1} \tag{64}$$

$$\mathbf{M}^{0}_{*\mathrm{e}} = \left(\left(\mathbf{P}^{0}_{\mathrm{e}}\right)^{-1} - \mathbf{C}_m\right)^{-1} \tag{65}$$

### 3.3. Elastic-viscoplastic cluster model

An additive interaction law can be conceptually formed by adding the elastic and viscoplastic interaction laws, Eq. (62) and Eq. (51). Considering that:

$$\mathbf{d}_I = \mathbf{d}_{\mathrm{e}}^I + \mathbf{d}_{\mathrm{v}}^I \tag{66}$$

and defining $\mathbf{d}_0$ by

$$\mathbf{d}_0 = \mathbf{d}_{\mathrm{e}}^0 + \mathbf{d}_{\mathrm{v}}^0 \tag{67}$$

we obtain:

$$\mathbf{d}_I - \mathbf{d}_0 = -\mathbf{M}_{*\mathrm{e}}^I \cdot (\dot{\boldsymbol{\sigma}}_I - \dot{\boldsymbol{\sigma}}_0) - \mathbf{M}_{*\mathrm{v}}^I \cdot (\mathbf{s}_I - \mathbf{s}_0) \tag{68}$$

where $\mathbf{M}_{*\mathrm{v}}^I$ and $\mathbf{M}_{*\mathrm{e}}^I$ are given by Eqs. (53) and (64).

In fact, this heuristically derived interaction law can be rationalized based on several arguments. Hashin (1969) found an analytical solution for the linear viscoelastic problem of a spherical inclusion embedded in an infinite matrix. The material response was of the Maxwell type in both phases and incompressibility was assumed. This solution can be exactly retrieved by using an additive interaction law having the same structure as Eq. (68), see Kouddane et al. (1993).

An additive interaction law was later proposed for solving inclusion problems, for non-linear, anisotropic, compressible material responses, including elasto-viscoplasticity, Molinari et al. (1997); Molinari, (2002). The instantaneous elastic response due to a jump in the external solicitation appears to be well restituted by this type of additive interaction law. On the other hand, for slow loading the quasi-nonlinear creep viscoplastic response is also well restituted. Moreover, it was verified by Mercier et al. (2005) that, for elastic-viscoplastic materials, the predictions of the additive interaction law for the single inclusion problem were in good agreement with Finite Element simulations for various loading conditions and strain paths.

Homogenization schemes have been proposed based on the additive form of the interaction law, Molinari et al. (1997), Abdul-Latif et al. (1998), Molinari (2002), Mercier and Molinari (2009), Kowalczyk-Gajewska and Petryk (2011), Abdul-Latif et al. (2018), Wang et al. (2010), Zecevic and Lebensohn (2020). These homogenization schemes have been validated by comparisons with Finite Element calculations (Mercier et al., 2012; Mercier et al., 2019) and experimental results (Girard et al., 2021).

Thus, it is appealing to extend the additive elastic-viscoplastic interaction law to account for the spatial distribution of inclusions in the framework of the interaction cluster model of Molinari and El Mouden (1996) and El Mouden and Molinari (2000).

Indeed, as for the interaction laws Eq. (62) and Eq. (51), all governing equations of the purely elastic and purely viscoplastic cluster models can be remarkably blended together within the additive formulation. Thus, the additive forms of Eq. (52) and Eq. (63) lead to:

$$\mathbf{D} - \mathbf{d}_0 = -\mathbf{M}_{*\mathrm{e}}^0 \cdot \left(\dot{\boldsymbol{\Sigma}} - \dot{\boldsymbol{\sigma}}_0\right) - \mathbf{M}_{*\mathrm{v}}^0 \cdot (\mathbf{S} - \mathbf{s}_0) \tag{69}$$

where $\mathbf{M}_{*\mathrm{e}}^0$ and $\mathbf{M}_{*\mathrm{v}}^0$ are given by Eq. (65) and (54).

Eq. (56) and Eq. (46) can be inverted into:

$$\mathbf{d}_{\mathrm{e}}^0 = \mathbf{M}_m \cdot \dot{\boldsymbol{\sigma}}_0 \tag{70}$$

$$\mathbf{d}_{\mathrm{v}}^0 = \mathbf{M}_m^{\mathrm{tg}} \cdot \mathbf{s}_0 + \mathbf{d}_m^{\mathrm{ref}} \tag{71}$$

with $\mathbf{M}_m = (\mathbf{C}_m)^{-1}, \mathbf{M}_m^{\mathrm{tg}} = \left(\mathbf{C}_m^{\mathrm{tg}}\right)^{-1}$ and $\mathbf{d}_m^{\mathrm{ref}} = -\mathbf{M}_m^{\mathrm{tg}} \cdot \mathbf{s}_m^{\mathrm{ref}}$. Combining Eq. (70) and Eq. (71) with Eq. (67), we obtain:

$$\mathbf{d}_0 = \mathbf{M}_m \cdot \dot{\boldsymbol{\sigma}}_0 + \mathbf{M}_m^{\mathrm{tg}} \cdot \mathbf{s}_0 + \mathbf{d}_m^{\mathrm{ref}} \tag{72}$$

With Eqs. (32,33), the linearized form of the matrix constitutive law reads:

$$\mathbf{d} = \mathbf{M}_m \cdot \dot{\boldsymbol{\sigma}} + \mathbf{M}_m^{\mathrm{tg}} \cdot \mathbf{s} + \mathbf{d}_m^{\mathrm{ref}} \tag{73}$$

Therefore, Eq. (72) shows that $\boldsymbol{\sigma}_0$ and $\mathbf{d}_0$ are related by the reference material response (matrix linearized law).

The macroscopic strain rate $\mathbf{D}(t)$ is assumed to be prescribed in terms of time (similarly one could assume the macroscopic stress $\boldsymbol{\Sigma}(t)$ to be prescribed). The relationship between $\mathbf{D}$ and microscopic strain rates reads:

$$\mathbf{D} = f\mathbf{d}_I + (1-f)\mathbf{d}_m \tag{74}$$

It is shown in Appendix B that Eq. (68), Eq. (69) and Eq. (74) constitute a linear system of first order differential equations for the stresses $\boldsymbol{\sigma}_I, \boldsymbol{\sigma}_m$ and $\boldsymbol{\sigma}_0$. These stresses appear to be the principal variables of the homogenization problem to which all other variables are subordinated.

## 4. Validation of the interaction cluster model by comparison with FE calculations

### 4.1. Basic configurations

The cluster model is applied here to two-phase composites. The elastic response of the phases is linear and isotropic. Therefore, the fourth order tensor of elastic compliance $\mathbf{M}$ involved in Eq. (1) is only related to the Young's modulus $E$ and Poisson's ratio $\nu$ of each phase. As in Lahellec and Suquet (2007), the viscoplastic behavior of each phase is governed by the Mises plasticity rule with a Norton flow stress:

$$\mathbf{d}_{\mathrm{v}} = \tilde{d}_0 \left(\frac{\sigma_{eq}}{\tilde{\sigma}_0}\right)^{\frac{1}{m}} \frac{3\boldsymbol{s}}{2\sigma_{eq}}, \quad \sigma_{eq} = \sqrt{\frac{3}{2}\boldsymbol{s}\cdot\boldsymbol{s}} \tag{75}$$

with $m$ the strain rate sensitivity parameter. Scalar parameters $\tilde{d}_0$ and $\tilde{\sigma}_0$ are reference strain rate and stress, respectively. In this work for model validation we concentrate on the linear case ($m = 1$) which is rich enough. The nonlinear case will be analyzed later. Three cases of matrix-inclusion setting in the composite have been selected, see Table 1.

Regular cubic (RC) and body centered cubic (BCC) spatial distributions of inclusions are adopted for evaluating the accuracy of the mean-field cluster model as compared to the results of full-field finite element (FE) simulations. Fig. 2 presents RC and BCC unit cells adopted in FE analysis for the volume fraction of inclusions $f = 0.25$. The size of the cubic unit cell is $a$, the radius of the inclusion, $R$. Note that for the same volume fraction and the same unit cell size $a$, the radius of the inclusion in the BCC unit cell is smaller than for RC: $R_{RC} = 2^{1/3} R_{BCC}$. Calculations were performed in AceFEM environment (Korelc, 2002) using 3D tetrahedral elements with 10 nodes. Periodic boundary conditions are prescribed at the external surface of the unit cells. Further details concerning FE calculations

**Table 1**
Elastic and viscous properties for the two phases. The matrix phase is viscoelastic. Three different configurations are considered for the inclusions. Case 1: hard elastic inclusion. Case 2: hard viscoelastic inclusion. The reference stress $\tilde{\sigma}_0$ will be varied in a large range of parameter $\eta > 1$. Case 3: Soft viscoelastic inclusion. The inclusion material properties ($E$ and $\tilde{\sigma}_0$) are derived from those ofvf the matrix with a scaling parameter $\zeta < 1$.

| | $E$ [GPa] | $\nu$ | $\tilde{\sigma}_0$ [MPa] | $\tilde{d}_0$ [1/s] |
|---|---|---|---|---|
| Viscoelastic matrix | 70 | 0.3 | 480 | 0.01 |
| Hard elastic inclusion (case 1) | 400 | 0.2 | – | – |
| Hard viscoelastic inclusion (case 2) | 400 | 0.2 | $480\eta$ | 0.01 |
| Soft viscoelastic inclusion (case 3) | $70\zeta$ | 0.3 | $480\zeta$ | 0.01 |

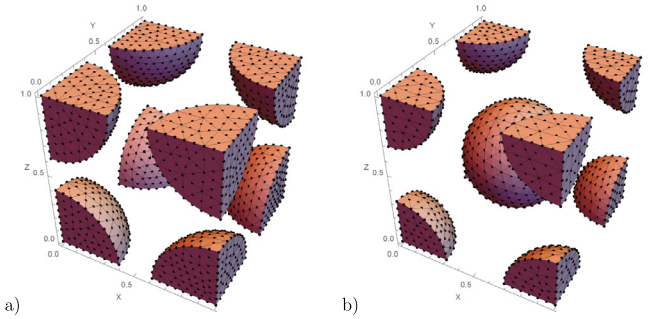


**Fig. 2.** a) Regular cubic (RC) and (b) body centred cubic (BCC) unit cells adopted in FE analysis (for better visibility FE mesh is displayed only for the inclusion phase). The volume fraction of inclusions is $f = 0.25$. The size of the cubic unit cell is $a$, the radius of the inclusions is $R$. Note that for the same volume fraction and the same $a$, the radius of the inclusions in the BCC unit cell is smaller than for RC.

and mesh generation can be found in Majewski et al. (2017) and Majewski et al. (2020).

### 4.2. Elastic inclusions

One of the goals of the present work is to increase the predicting capability of mean field approaches for composite materials with elastic inclusion and viscoelastic or viscoplastic matrix. An interesting trend was depicted in Lahellec and Suquet (2007) and Czarnota et al. (2015), where some large discrepancy was observed between the Mori-Tanaka approach (MT) and full field simulations obtained by FFT or FEM calculations in the case of elastic inclusion with linear viscoelastic matrix. For the full-field calculations, material parameters of the matrix linear viscoelastic response and for the linear elastic response of inclusions were those given in Table 1, Case 1. The volume fraction of inclusions was $f = 0.25$. Under uniaxial tension at a longitudinal strain rate of $10^{-2}s^{-1}$ and for a random distribution of inclusions dispersed in the matrix, Czarnota et al. (2015) observed that the prediction in terms of uniaxial stress captured by the MT scheme underestimated the FE results by around 25% (when $m = 1$). It was also observed that as $m$ was decreased, the predictions of the MT scheme were more and more accurate in terms of overall stress, see Fig. 6a) of Czarnota et al. (2015). It was also seen that for a lower volume fraction of inclusion $f = 0.1$, the match for $m = 1$ was more precise. Therefore the authors were considering that the discrepancy between FE results and homogenization technique was mostly inherited from the averaging scheme. Note that the same configuration was previously proposed by Lahellec and Suquet (2007). Full-field calculations were performed with the FFT approach. The homogenization procedure was carried out with the *EIV* + *HS*

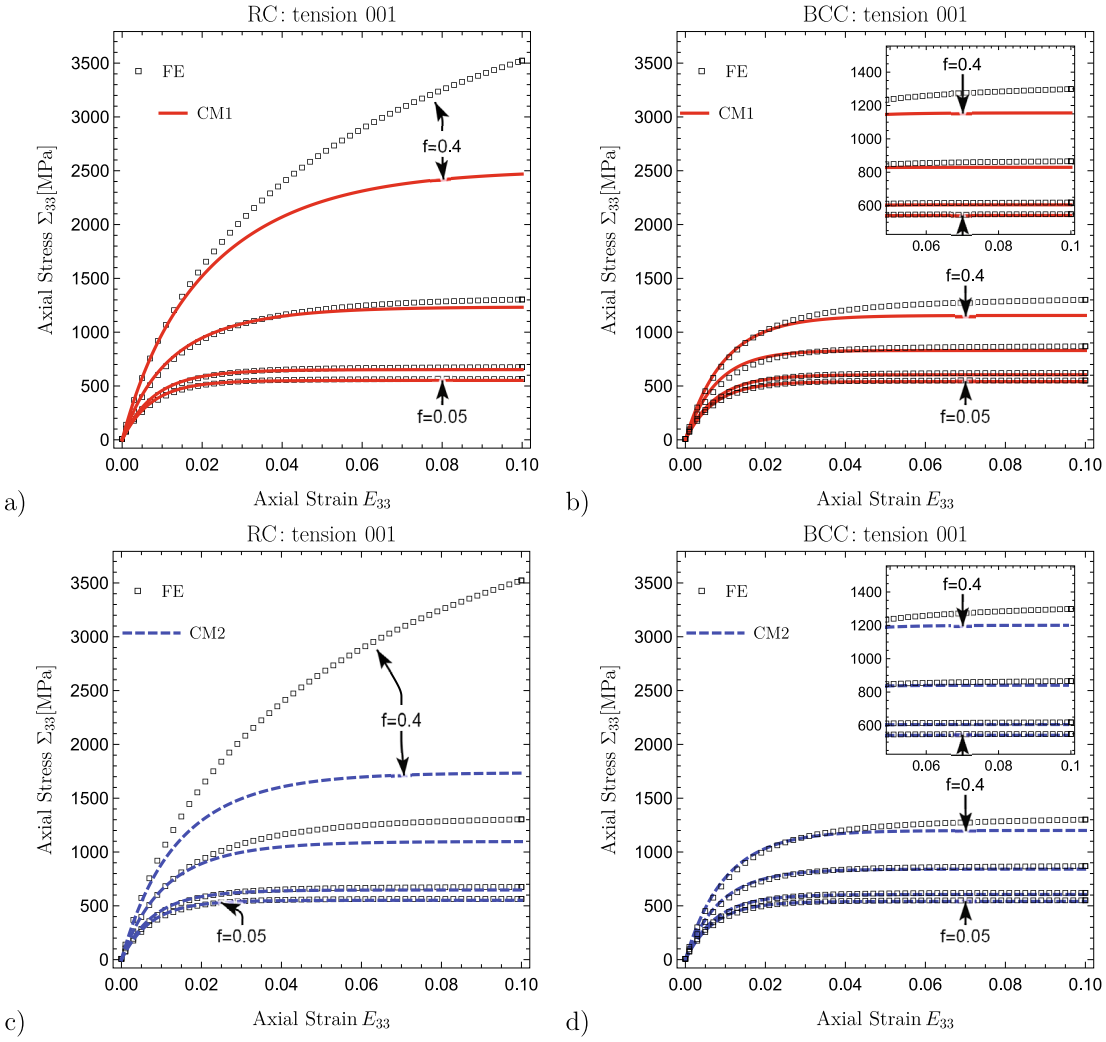


**Fig. 3.** Overall axial stress-strain response for uniaxial tension along (001) direction. Predictions of a) CM1 model with a RC configuration, b) CM1 model with a BCC configuration, c) CM2 model and a RC configuration, d) CM2 model and a BCC configuration. The matrix has a viscoelastic response: $E_m = 70$ GPa, $\nu_m = 0.3$, $\bar{\sigma}_0^m = 480$ MPa and $\bar{d}_0 = 0.01$ s$^{-1}$. The strain rate sensitivity is $m = 1$ (linear viscoelasticity). Hard elastic inclusions are considered with $E_I = 400$ GPa and $\nu_I = 0.2$ (case 1 of Table 1). Different volume fractions of inclusions are considered: $f = \{0.05, 0.1, 0.25, 0.4\}$. The predictions of the two cluster models CM1 and CM2 are compared to finite element results.

method (secant linearization and Hashin-Strickman bound). Similar discrepancy on the overall stress was found (around 25%). Note that in the two examples, the inclusions were randomly and isotropically distributed. With the viscoelastic cluster model, the effects due to interaction between inclusions and to particle packing are accounted for. Therefore, as compared to the Mori-Tanaka approach a much better prediction of the overall response is expected, especially in the critical case where $m = 1$. Closer predictions than Mori-Tanaka approach could be obtained. Validation of the cluster model for linear viscoelasticity is conducted in the following of this section.

Fig. 3 presents the overall axial stress-strain response during a (001) uniaxial tension. The volume fraction of inclusion is varying from $f = 0.05$ to $f = 0.4$. The predictions of the cluster model CM1 for the RC configuration are displayed in Fig. 3 a) and for BCC in Fig. 3 b). The predictions of the hybrid model CM2 are presented in Fig. 3 c) for a RC array and in Fig. 3 d) for BCC array. FEM predictions are also displayed in all figures. A clear effect of the topology is observed as the stress-strain curves for RC and BCC configurations are different. This is more marked as the volume fraction of inclusions increases. From FE calculations, it is seen that in the case of the RC geometry, the uniaxial stress reaches almost 3500 MPa at 0.1 uniaxial strain, while its value is lower than 1500 MPa for the BCC geometry. For the RC configuration, the cluster model CM1 is capable of accurate predictions up to $f = 0.25$ and up to $f = 0.2$ for the CM2 approach. For the BCC configuration, the results are still of good quality up to $f = 0.3$ for both models CM1 and CM2. Comparing results of CM1 and CM2 models allows to evaluate the interaction effect between inclusions. With Eqs. (29) and (28) it has been demonstrated that CM1 provides stronger interaction effects than CM2. This is confirmed and quantified by the results of Fig. 3. In the following, only predictions for $f = 0.1$ and $f = 0.25$ will be adopted.

Fig. 4 gathers in a more concise way, results of Fig. 3, where the composite is facing uniaxial tension in the (001) direction. A comparison is presented between stress-strain curves evaluated by the two cluster approaches and FE predictions, for two selected volume fractions $f = 0.1$ and $f = 0.25$. In addition results obtained with the Mori-Tanaka approach for elastic-viscoplastic materials (Mercier and Molinari, 2009; Kowalczyk-Gajewska and Petryk, 2011) are also depicted. For a BCC arrangement of inclusions, predictions of the three models (MT + Cluster models CM1 and CM2) are quite accurate even for the largest volume fraction, see Fig. 4 b) and d). More interesting is the analysis of results for the RC array. Even for the lowest volume fraction of inclusions, one observes a significant effect on the axial stress-strain curve of the adopted

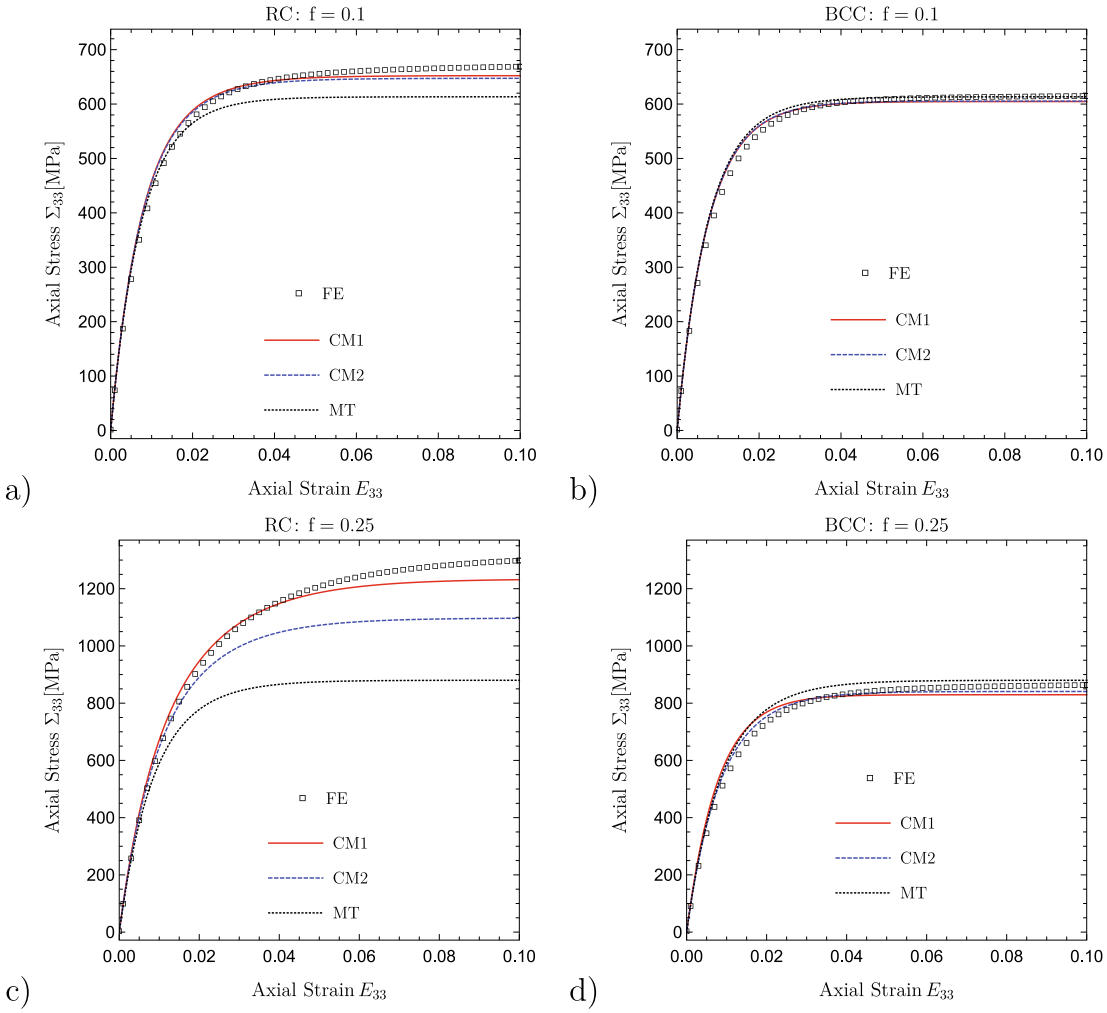


**Fig. 4.** Overall axial stress-strain response of a two-phase composite for a uniaxial tension along (001) direction. Predictions of the two cluster approaches CM1 and CM2 and of the Mori-Tanaka approach are compared to finite element simulations for: a) volume fraction $f = 0.1$ and RC array, b) $f = 0.1$ and BCC array, c) $f = 0.25$ and RC array, d) $f = 0.25$ and BCC array. Inclusions are elastic and the matrix has a linear viscoelastic behavior (of the Maxwell type). Material parameters are those of Fig. 3, see Table 1, Case 1.

modeling route: *i.e.* the two cluster models versus the classical Mori-Tanaka approach. Remember that the present Mori-Tanaka scheme can be retrieved from the cluster models by considering a cluster of zero radius ($R_c = 0$), with the effect of much decreasing the particle interaction. The MT approach is providing a poor estimate of the overall stress level. For this volume fraction and the adopted material parameters, an impact of the interactions between inclusions is significant. As a consequence, the new cluster approach provides a clear improvement of the predictions. Furthermore, the cluster model CM1 generates better agreement when compared to the cluster model CM2. This result is really an important outcome of the present paper. Fig. 4 provides also an illustration of the hierarchy between CM1, CM2 and MT models, from larger to lower effect of particle interactions. Thus, it is clearly seen in Fig. 4, that the effective response of the composite is better described with the higher interaction effect carried by CM1. It clearly shows that for elastic inclusions and linear viscoelastic matrix, the interactions between inhomogeneities are a key feature, which need to be integrated in the model. Therefore, the present work sheds light on why a strong difference was observed in Lahellec and Suquet (2007) and Czarnota et al. (2015) when the composite was made of elastic inclusion and linear viscoelastic matrix. Configurations for non-linear behavior ($m < 1$) will be investigated in a future work.

It is also of interest to investigate how local mechanical fields are captured. Fig. 5 presents the average local axial stress $\sigma_{33}$ versus axial strain $\epsilon_{33}$ in both phases. The overall response is also displayed as a supplementary information. The hard inclusion phase shows a stiff elastic response, while the stress-strain response is non-linear in the matrix phase due to its viscoelastic behavior. It is observed that for $f = 0.1$, the stress-strain levels given by the two cluster models are in close agreement with the numerical results. The large dots in Fig. 5 (blue color for Cluster CM2, red for cluster CM1 and black for FE) indicate the average stress-strain fields at the intermediate overall axial strain $E_{33} = 0.05$ and at the end of the deformation process (when the overall axial strain is equal to 0.1). It is interesting to observe that the stress or strain levels in the inclusion for overall strain $E_{33} = 0.05$ or $E_{33} = 0.1$ are similar, meaning that for this configuration (elastic inclusion and linear viscoelastic matrix), the overall deformation is mostly accommodated by the matrix phase for $E_{33} > 0.05$. For the BCC array, the three modeling routes lead to almost identical predictions. A slight difference is seen in favour of CM1 approach for the RC array, see Fig. 5a). The strain in the inclusion is

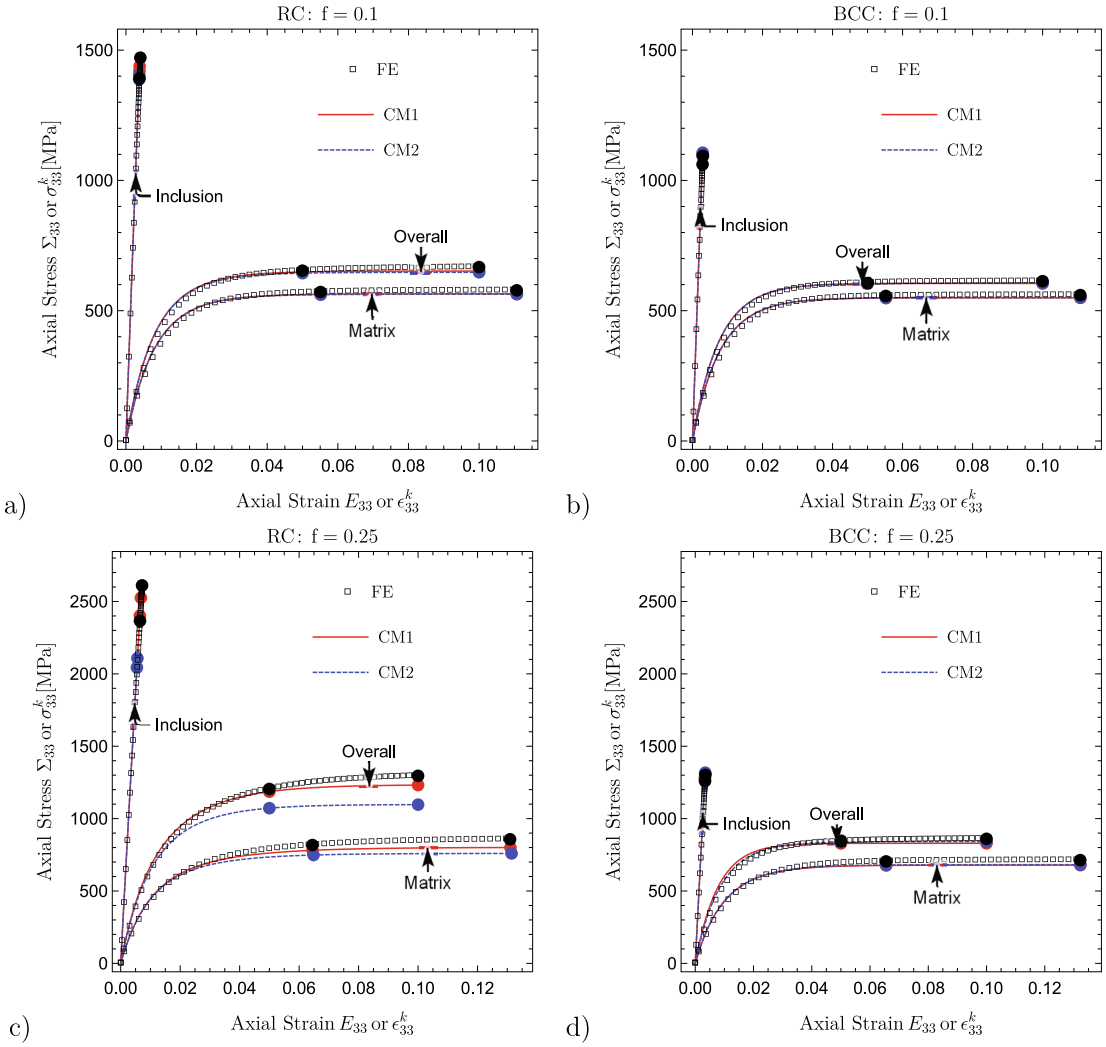


**Fig. 5.** Overall and local axial stress versus axial strain during uniaxial tension along (001) direction. Predictions of the two cluster models are compared to average values captured by finite element calculations: a) RC unit cell with $f = 0.1$, b) BCC unit cell with $f = 0.1$, c) RC unit cell and $f = 0.25$ and d) BCC unit cell and $f = 0.25$. Inclusions are elastic and linear viscoelasticity is considered for the matrix. Material parameters are those of Fig. 3 and listed in Table 1, Case 1. Note that large dots mark the stress and strain level at an intermediate overall strain $E_{33} = 0.05$ and at the end of the deformation process $E_{33} = 0.1$.

underestimated, with a slightly better predictions for the cluster CM1 approach. For the largest volume fraction of inclusion $f = 0.25$, it is important to notice that the local response is also accurately predicted for a BCC array. For RC array and $f = 0.25$, the mismatch observed for the overall prediction is also present for the average fields in the two phases. A better agreement is found for the cluster approach CM1. We have checked that the presented results are not influenced by a larger cluster radius (here we used $R_c = 8d$, with $d$ the minimum distance between centers in the unit cell size). Therefore, a possible explanation could be the non-homogeneous strain field in the inclusion which becomes more pronounced for large volume fraction of inclusions.

The difference between RC and BCC arrays is due to packing effect. Let us define for the RC array, the directional compacity index $\lambda_{RC}^{001} = \frac{R}{d_{RC}^{001}}$ as the ratio of the inclusion radius $R$ to the distance between two centers of the closest inclusions $d_{RC}^{001}$, this distance being measured in the loading direction (001). It is easily seen from Fig. 2a, that $\lambda_{RC}^{001} = \frac{R}{a} = \left(\frac{3f}{4\pi}\right)^{1/3}$. For the BCC configuration, the same ratio is $\lambda_{BCC}^{001} = \frac{R}{a} = \left(\frac{3f}{8\pi}\right)^{1/3}$. For the same volume fraction this ratio is larger than for RC, meaning that inclusions are closer (relatively to the radius) for RC array than for BCC. Thus, for the (001) loading direction, the interaction between inclusions is stronger for the RC array. As hard inclusion is considered in this first series of calculations, the overall stress level is also larger for RC than for BCC. Note that inclusions are touching each other for $\lambda_{RC}^{001} = 0.5$ or equivalently for $f = 0.52$. Such condition can not be satisfied for BCC configuration. Indeed, the compacity of the unit cell is reached for $f = 0.68$, corresponding to $\lambda_{BCC}^{001} = 0.348$. An alternative volumic (not directional) compacity index would be $\frac{R}{d}$, with $d$ being the closest distance between inclusion centers. But this volumic index would not explain the difference of results related to the direction of loading.

Next, the effect of the loading direction is investigated to demonstrate the capability of the scheme to reproduce anisotropy of the overall response inherited from the topological arrangement of inclusions. Of course, such property cannot be reproduced by the classical Mori-Tanaka scheme. For that purpose, an isochoric tension process is adopted instead of uniaxial tension (as in the previous calculations):

$$\mathbf{D} = \dot{\bar{\varepsilon}}/2(3\mathbf{k}\otimes\mathbf{k} - \mathbf{I}), \tag{76}$$

where the unit vector $\mathbf{k}$ corresponds to the loading direction. In the following, the cell diagonal direction (111) or the direction (001) will be considered only. The equivalent strain rate $\dot{\bar{\varepsilon}}$ is set to $10^{-2}$ s$^{-1}$. Fig. 6 presents the stress-strain response for a volume fraction of inclusion varying from $f = 0.05$ to $f = 0.4$ and (111) direction. The predictions of the cluster model (CM1) for the RC configuration are displayed in Fig. 6a) and for BCC in Fig. 6b). We observe that the CM1 cluster model provides efficient estimates up to 0.2 volume fraction of inclusion for BCC array and 0.4 for RC array. This observation is exactly reversed when compared to results of Fig. 3 (note that the response in isochoric tension in (001) direction is qualitatively similar to the response in uniaxial tension in the same direction studied previously). To understand this trend, one should compare the directional compacity indexes which are now $\lambda_{RC}^{111} = \frac{1}{\sqrt{3}}\left(\frac{3f}{4\pi}\right)^{1/3}$ and $\lambda_{BCC}^{111} = \frac{1}{\sqrt{3}}\left(\frac{3f}{\pi}\right)^{1/3}$. Therefore one has $\lambda_{RC}^{111} < \lambda_{BCC}^{111}$. Inclusions are relatively closer in the (111) loading direction for BCC array than for RC one. Thus the interaction between inclusions is more pronounced for BCC. The heterogeneity within the inclusion is enhanced leading to larger discrepancy between the predictions and the FE calculations when the volume fraction of inclusions becomes large. In addition, as inclusions (hard phase here) are directionally closer in the BCC cell, the overall stress level $\mathbf{k}.\boldsymbol{\Sigma}.\mathbf{k}$ is larger for the BCC configuration than for RC when $\mathbf{k}$ is parallel to (111).

Fig. 7 presents the local axial stress $\mathbf{k}.\boldsymbol{\sigma}.\mathbf{k}$ and strain $\mathbf{k}.\boldsymbol{\epsilon}.\mathbf{k}$ (in the (111) direction) for two volume fractions $f = 0.1$ and $f = 0.25$. As the overall response was perfectly captured for the two RC and BCC arrays and for the low volume fraction $f = 0.1$, see Fig. 6, the local response in the matrix and in the inclusion appears to be sufficiently well predicted too, at least on average. The stress in the inclusion is only slightly underpredicted. For $f = 0.25$ and the RC unit cell, the overall stress-strain curve is well captured by the two cluster models. This is also the case at the scale of individual phases. For the BCC case and $f = 0.25$, the mismatch between cluster models and FE results is mostly caused by the limited capability of capturing in a proper manner the average value of the strain and stress in the inclusion domain. Among all configurations of this figure, the directional compacity index for

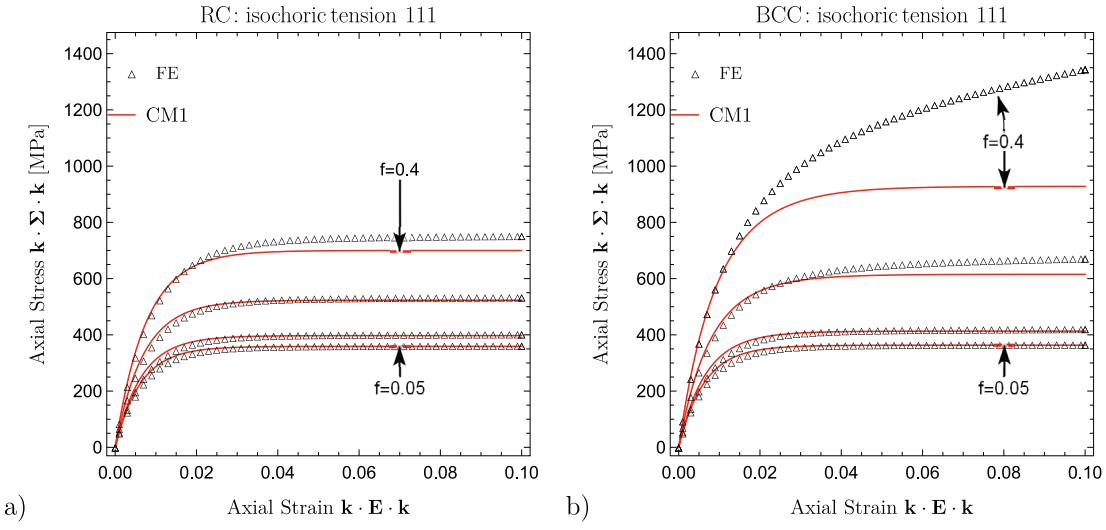


**Fig. 6.** Overall axial stress-strain response for isochoric tension along (111) direction. Predictions of a) CM1 model with RC configuration, b) CM1 model with BCC configuration are compared to finite element results. The matrix has a linear viscoelastic response. Hard elastic inclusions are considered. Material parameters are provided in Table 1, case 1. Different volume fractions of inclusions are adopted: $f = \{0.05, 0.1, 0.25, 0.4\}$.

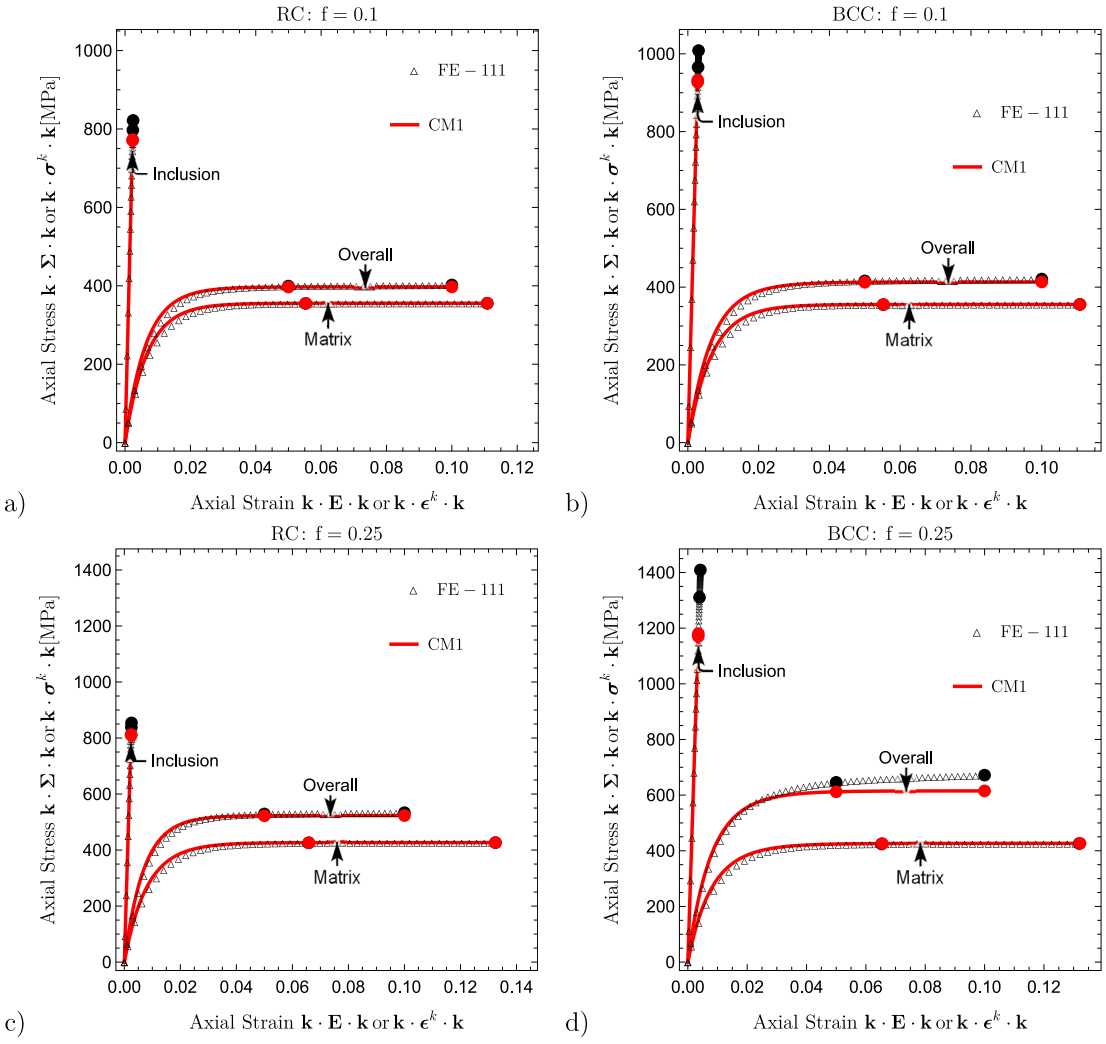


**Fig. 7.** Overall and local axial stress – axial strain response during isochoric tension along (111) direction. Predictions of the cluster model CM1 are compared to average values captured by finite element calculations: a) RC unit cell with $f = 0.1$, b) BCC unit cell with $f = 0.1$, c) RC unit cell and $f = 0.25$ and d) BCC unit cell and $f = 0.25$. Inclusions are elastic and linear viscoelasticity is considered for the matrix. Material parameters are those of Fig. 3 or listed in Table 1, case 1. Note that large dots mark the axial stress and strain level at the overall axial strain $\mathbf{k}\cdot\mathbf{E}\cdot\mathbf{k} = 0.05$ and at the end of the deformation process $\mathbf{k}\cdot\mathbf{E}\cdot\mathbf{k} = 0.1$. In the present calculations, $\mathbf{k}$ is the unit vector parallel to (111) direction.

this case (BCC and $f = 0.25$) is the largest: $\lambda^{111}_{BCC} = 0.358$. Therefore, the interactions between inclusions are strong, and the associated heterogeneity in strain field is the largest.

Fig. 8 exemplifies the intensity of the topology-induced anisotropy on the overall response when the volume fraction and the packing are varied. For that purpose, two volume fractions ($f = 0.1$ and $f = 0.25$) are considered as well as the two geometrical configurations: RC and BCC arrays. Isochoric tensions along (001) and (111) directions are prescribed to the composite material. The predictions of the cluster model CM1, of the MT scheme and FE results are displayed in Fig. 8. For $f = 0.1$, almost no difference in the response for the two directions is observed for the BCC cell and limited anisotropy is seen for the RC one. Indeed, the directional compacity index is: $\lambda^{111}_{BCC} = 0.26, \lambda^{111}_{RC} = 0.166, \lambda^{001}_{BCC} = 0.23$ and $\lambda^{001}_{RC} = 0.288$, respectively. The variation of $\lambda$ is more pronounced for the RC array, leading to stronger anisotropy. Results allow to say that when the index is lower or around 0.3, the cluster model and FE predict similar results. Trends are confirmed for $f = 0.25$. In that case, the four indexes are: $\lambda^{111}_{BCC} = 0.358, \lambda^{111}_{RC} = 0.22, \lambda^{001}_{BCC} = 0.31$ and $\lambda^{001}_{RC} = 0.382$, respectively. Note also that as the index is approaching the critical value of 0.5 (in that configuration, inclusions are touching each other), inclusions become so close that strong interaction effects are produced. This is the case for RC and (001) direction, where the MT approach cannot capture this strong interaction effect. Only the cluster CM1 can provide reasonable predictions. This effect was discussed earlier in the paper, and already observed for isotropic distribution of inclusions in Lahellec and Suquet (2007) and Czarnota et al. (2015). It is also interesting to observe that the Mori-Tanaka approach provides good agreement for the loading direction presenting the lowest directional compacity index, *i. e.* (111) direction for RC array and (001) direction for BCC array.

### 4.3. Viscoelastic inclusions

In this subsection, both phases (inclusion and matrix) have viscoelastic behavior. The matrix material parameters are the same as in the previous Section 4.2 and given in Table 1.

#### 4.3.1. Hard inclusions

In this section, the case of hard viscoelastic inclusions in a viscoelastic matrix is investigated. Material properties of inclusions are provided in Table 1, Case 2. It is seen that the elastic properties of the inclusion are similar to the previous Section 4.2, but the

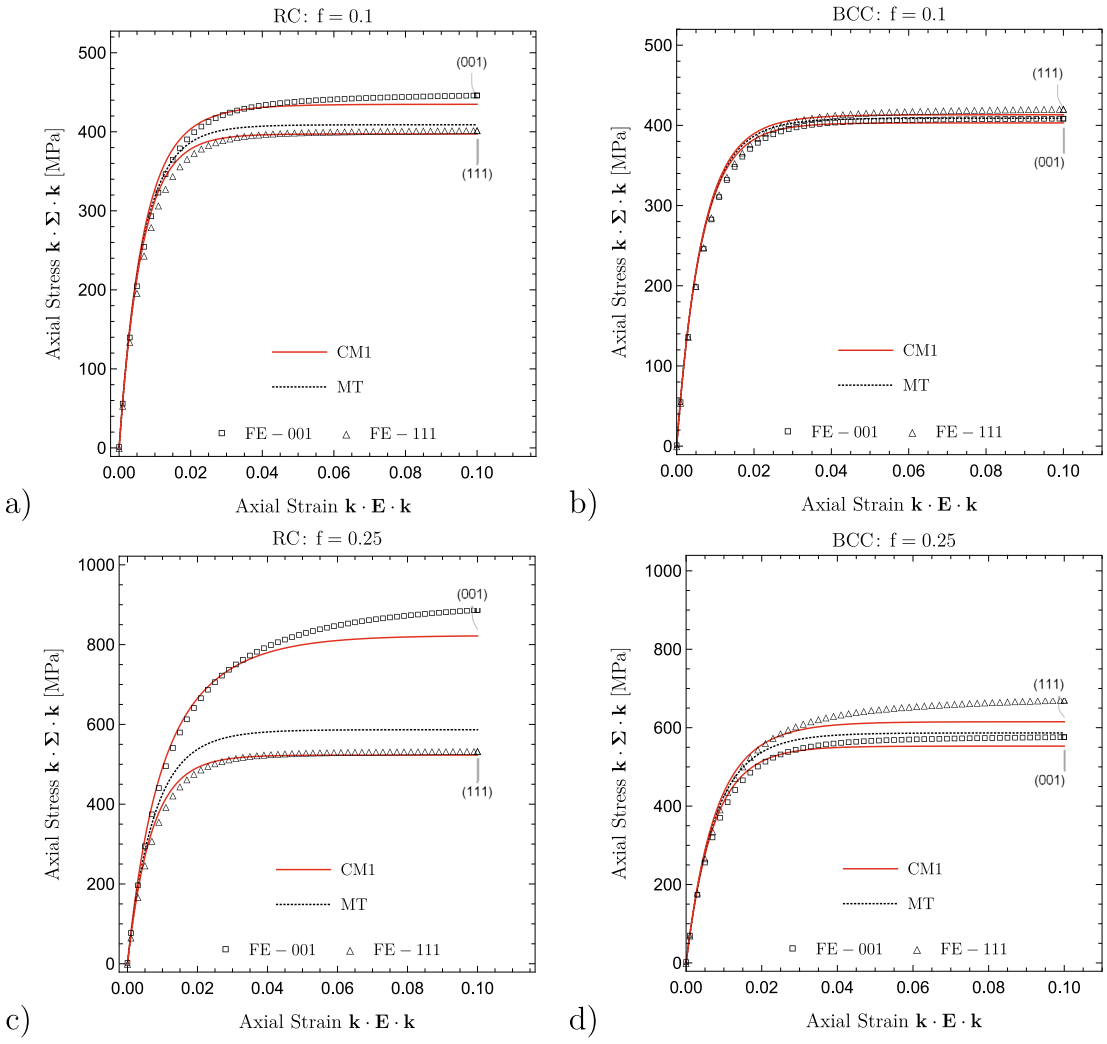


**Fig. 8.** Comparison of the overall stress-strain response during isochoric tension along (111) and (001) directions. The topology-induced anisotropy is illustrated for: a) $f = 0.1$ and RC array of inclusions, b) $f = 0.1$ and BCC array of inclusions, c) $f = 0.25$ and RC array, d) $f = 0.25$ and BCC array. Predictions of the cluster model CM1, of the Mori-Tanaka approach and of finite element calculations are compared. Inclusions are elastic and linear viscoelasticity is considered for the matrix. Material parameters are those of Fig. 3 or listed in Table 1, case 1.

viscous response of the inclusion phase is parametrized by the coefficient $\eta > 1$. With the proposed definition, the inclusion phase is still the hard one, but with a more or less pronounced viscous contribution depending on the value of $\eta$. Note that the case 1 (elastic inclusion) depicted in the previous section is recovered when $\eta$ tends to $\infty$. The volume fraction is set to $f = 0.25$. Uniaxial tension along (001) direction is only considered.

Effective responses are first provided for RC and BCC unit cells in Fig. 9a) and b). It is seen that for both arrangement of inclusions, the prediction of the cluster model is consistent with the FE predictions in the considered range of viscous parameter ($\eta$ takes values: $2, 5, 10$); the parameter $\tilde{\sigma}_0^I$ being in the range [960–4800] MPa. As the viscous parameter of the inclusion is larger, the inclusion response is closer to an elastic one. Therefore, some mismatch between the CM1 model prediction and numerical one is retrieved. This is more visible for the RC array, where the directional compacity index is larger ($\lambda_{RC}^{001} = 0.382$ and $\lambda_{BCC}^{001} = 0.31$).

Interestingly, it has been checked that overall stress-strain responses are also accurately predicted by the CM1 model for a volume fraction of $f = 0.4$ and $\tilde{\sigma}_0^I = 2400$ MPa. Therefore depending on the constitutive law of the two phases, introducing the interaction between inclusions in the modeling may be sufficient to propose consistent results for large volume fraction of inclusions.

Fig. 9c) and d) compare the average local stress-strain response in each phase for the two configurations RC and BCC. The $\eta$ parameter is set to 10 ($\tilde{\sigma}_0^I = 4800$ MPa). For BCC array, it is seen in Fig. 9d) that all modeling routes (cluster model CM1 + MT + FE) provide consistent results for the overall composite but also for average fields in the matrix phase. Concerning the inclusion phase, the average axial stress level predicted by the MT approach is too large while the cluster CM1 is well capturing this level. For the RC configuration, the predicting capability of the CM1 approach is still excellent for the overall response and also at the phase level. One observes that the MT approach significantly underestimates the overall stress level. Clearly, with the proposed figure, as the interaction between inclusion becomes more intense, the need for a more advanced model, as the cluster model, is compulsory. One can also mention that the viscoelastic transition in the FE calculations is more progressive than in the predictions based on CM1 model. This evidences the heterogeneity of the strain field in the inclusion domain. An extension of the cluster model accounting for second order moment could be a strategy to be tested in a near future.

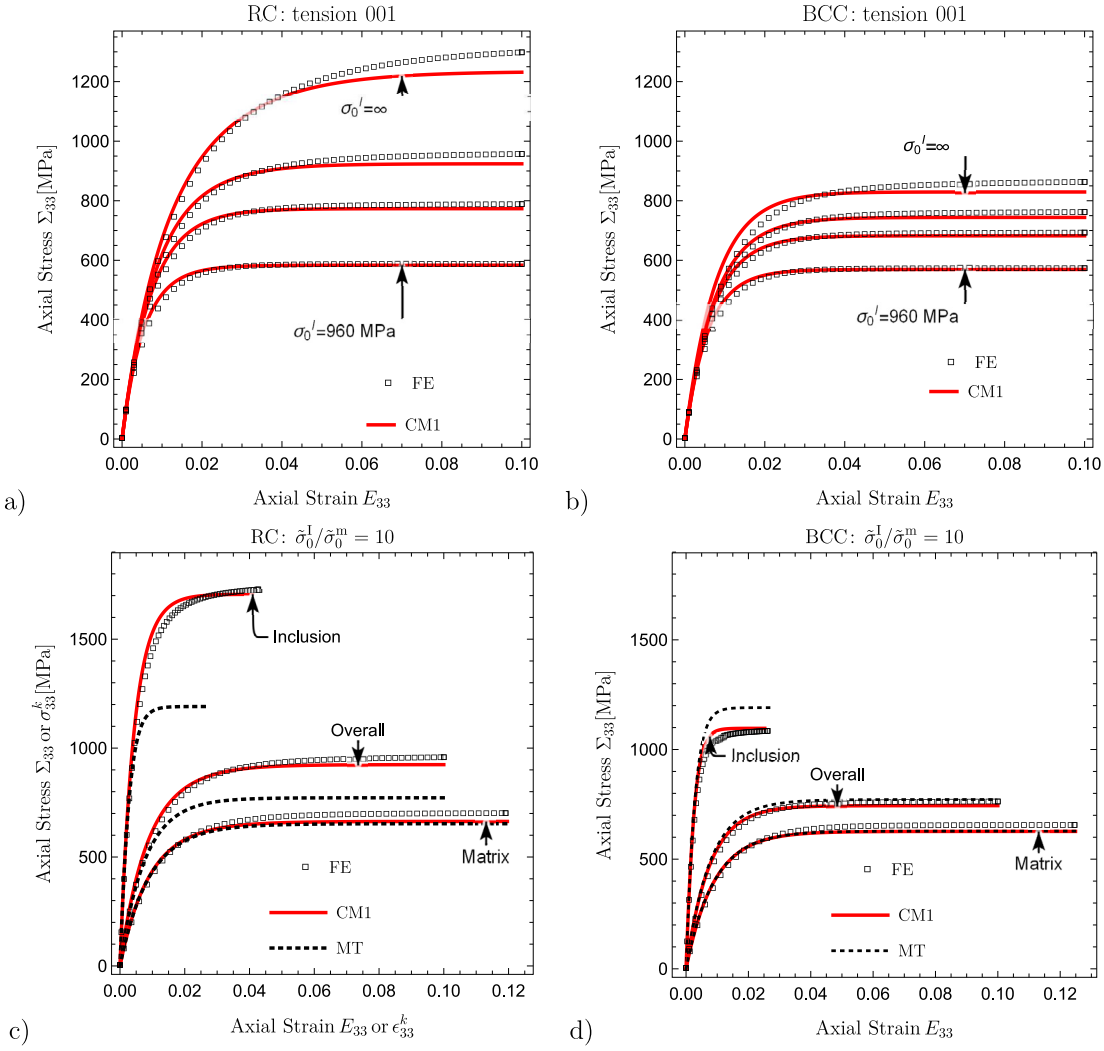


**Fig. 9.** Overall axial stress-strain response in uniaxial tension along (001) direction of a) RC array, b) BCC array. Both phases have viscoelastic behavior. The inclusion phase is the hard one. The viscous stress parameter $\tilde{\sigma}_0^I$ of the inclusion takes values: 960, 2400, 4800 MPa. The case of elastic inclusion is also added ($\eta = \infty$). Local and overall axial stress-strain response for $\tilde{\sigma}_0^I = 4800$ MPa and c) RC array, d) BCC array. The predictions of the cluster model CM1, of the Mori-Tanaka approach for elastic-viscoplastic materials and of FE are compared. Material properties except $\tilde{\sigma}_0^I$ are provided in Table 1, Case 2. The volume fraction of inclusions is $f = 0.25$.

*4.3.2. Soft inclusions*

In the last example, we consider soft inclusions, case 3 of Table 1. The matrix phase is kept identical as in the two previous examples, see for instance Section 4.2. In this part, to soften the inclusion behavior, a parameter $\xi$ is introduced to scale both the Young's modulus and the viscous stress parameter $\tilde{\sigma}_0^I$. In the present paper, the condition $\xi < 1$ is enforced. Note that for $\xi = 1$, inclusion and matrix phases have identical behavior and the composite is homogeneous.

Fig. 10 a) and b) presents the overall predictions given by the CM1 cluster model and FE calculations. The parameter $\xi$ takes values: $1/2, 1/5, 1/10$ (*i.e.* $\tilde{\sigma}_0^I = 240, 96, 48$ MPa). For all the cases and for the two packing arrangements RC or BCC, the agreement is accurate between predictions of CM1 and FE routes. Results of the MT approach are presented only for the softer case $\xi = 1/10$ or $\tilde{\sigma}_0^I = 48$MPa in Fig. 10c) and d). For BCC array, the MT approach provides similar overall response as the one given by CM1 and FE models. For the RC array, the MT scheme leads to an underestimation of the overall stress level.

Even if the overall response is accurate, it is seen that at the level of phases, the situation is different. Fig. 10c) and d) depict a situation where the magnitude of the average strain in the inclusion is quite satisfactorily predicted by the CM1 model but the corresponding average stress level in the inclusion is clearly underestimated for RC and BCC arrays. For the MT approach, one observes that the average strain in the inclusion is really too large for the RC configuration, leading to an underestimation of the strain level in the matrix phase also. For the BCC one, the situation is reversed with a small strain amplitude in the inclusion phase.

Finally, the anisotropy induced by the inclusion arrangement is also tested for soft inclusions, see Figure 11. For illustrative purpose, the parameter $\xi = 1/10$ is prescribed and the volume fraction of inclusions is $f = 0.25$. In this example, the composite is subject to isochoric tension, as described in Eq. (76) with the equivalent plastic strain rate $\dot{\bar{\varepsilon}} = 10^{-2}$ s$^{-1}$. The two directions (001) and (111) are selected. Remember that the directional compacity indexes are: $\lambda_{BCC}^{111} = 0.358, \lambda_{RC}^{111} = 0.22, \lambda_{BCC}^{001} = 0.31$ and $\lambda_{RC}^{001} = 0.382$. For the BCC configuration, the two indexes are quite similar and as a consequence, limited anisotropy is obtained. This trend captured by FE calculations is well reproduced by the cluster model CM1. Note also that the Mori-Tanaka approach is providing satisfactorily predictions. For the RC array, the uniaxial response is clearly direction dependent. Indeed, the distance between neighbouring inclusions is varying with the loading direction, so is the

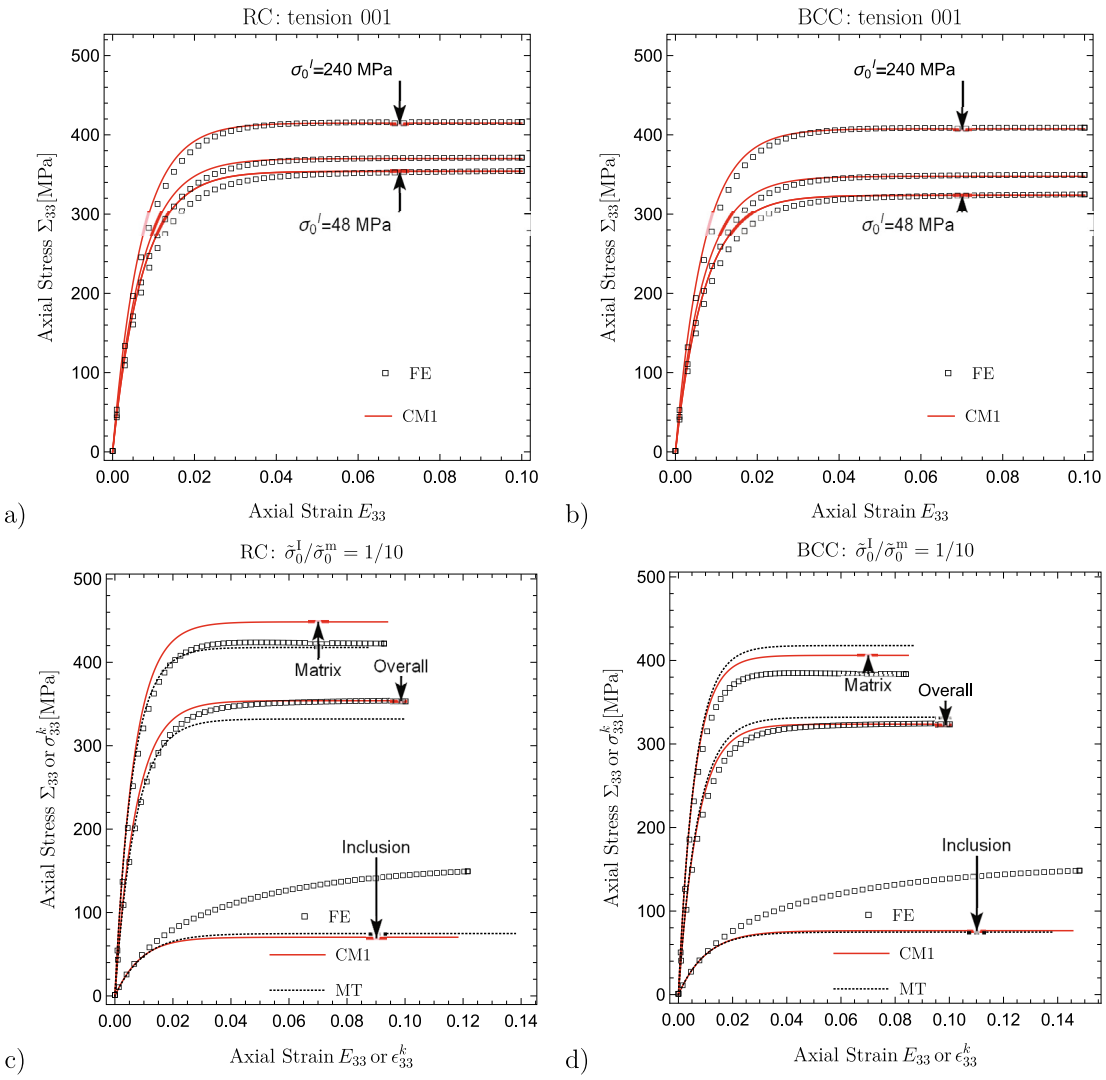


**Fig. 10.** Overall axial stress versus axial strain in uniaxial tension along (001) direction of a) RC array, b) BCC array. Both phases have viscoelastic behavior. The inclusion phase is the soft one. The viscous stress parameter $\tilde{\sigma}_0^I$ of the inclusion takes values: 48, 96, 240 MPa and Young's modulus is 7, 14, 35 GPa, correspondingly. Local and overall axial stres versus strain response for $\tilde{\sigma}_0^I = 48$ MPa, $E_I = 7$ GPa and c) RC array, d) BCC array. The predictions of the cluster model (CM1), of the Mori-Tanaka approach for elastic-viscoplastic materials and of FE are compared. Material properties are provided in Table 1, Case 3. The volume fraction of inclusions is $f = 0.25$.

directional compacity index $\lambda$ (0.22 for (111) and 0.382 for (001)). In this figure, it is shown that the cluster model can capture with a good accuracy the FE results, also when soft inclusions are considered. In that case, the Mori-Tanaka model is capturing an intermediate response.

## 5. Conclusions

A mean field interaction model has been proposed for describing the global response of an elastic-viscoplastic composite and for estimating the average stresses and strains per phases. The present work appears as an extension to elasto-viscoplasticity of the mean field interaction model (known also as cluster model) originally developed for linear thermoelasticity.

A two-phase composite made up of inclusions embedded in a uniform matrix is considered. The main features of the model are the following:

(i) Topological aspect: the spatial distribution of phases is accounted for.
(ii) Morphological aspects: shapes of inclusions are considered (ellipsoidal shape).
(iii) Material aspects: phases are governed by non-linear Maxwell laws with hardening.
(iv) The tangent linearization of non-linear viscoplastic laws (Molinari et al., 1987) is used to formulate interaction laws.
(v) Interactions between phases are described by using the concept of additive interaction laws where elastic and viscoplastic response are blended together. Such laws provide relationships between local fields (intra-phase) and macroscopic fields.
(vi) The time evolution problem is reduced to solving a system of first order differential equations.

The proposed approach has been validated by comparison with unit-cell Finite Element simulations. Although the model was presented for non-linear Maxwell type responses, applications were focused here on the linear viscoelastic case which by itself provides a rich field of investigations. Applications to non-linear responses is the object of future developments. For illustration, simple internal structures were considered: a single family of inclusions spatially distributed according to a BCC or a RC array. Generalization to more complex internal structures can be achieved by following the lines proposed by Molinari and El Mouden (1996) for elastic

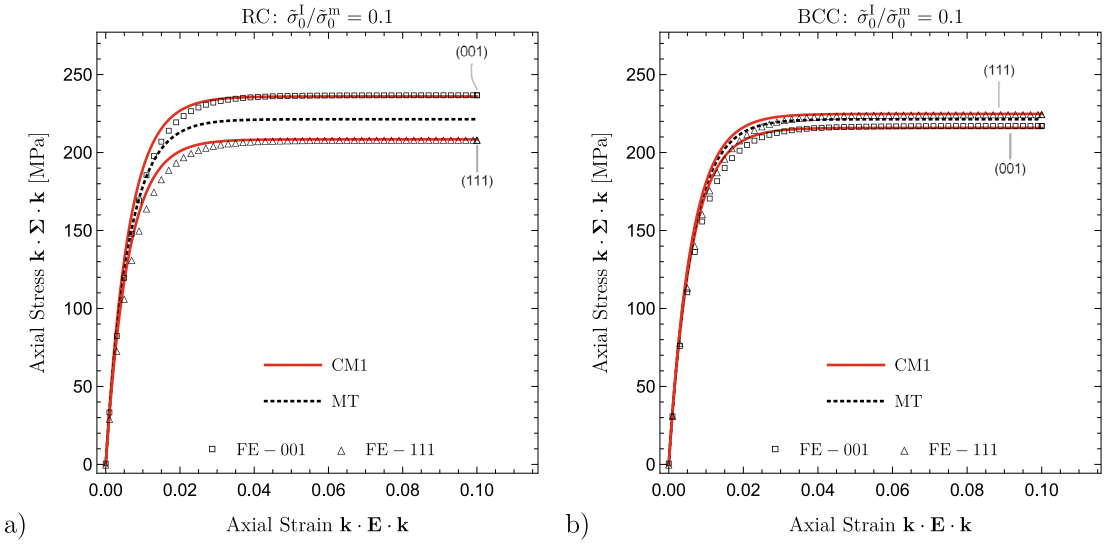


**Fig. 11.** Comparison of the overall axial stress versus axial strain during isochoric tension along (111) and (001) directions. The induced anisotropy is illustrated for: a) RC array of inclusions, b) BCC array of inclusions. Predictions of the cluster model (CM1), of the Mori-Tanaka (MT) approach and of finite element calculations are compared. The volume fraction of inclusions is $f = 0.25$. Inclusion and matrix phases have a linear viscoelastic behavior, with material parameters listed in Table 1, Case 3. Inclusion is the soft phase. The viscous stress parameter and Young's modulus for the inclusion phases are set to $\bar{\sigma}_0^I = 48$ MPa and $E_I = 7$ GPa.

composites. The approach can be also adopted to study random distributions described by a given probability density function.

The viscoelastic case is known to offer difficulties when treated with available approaches, see e.g. Czarnota et al., 2015; Lahellec and Suquet, 2007, especially when elastic inclusions of finite volume fraction are embedded in a viscoelastic matrix. As concerns material properties of inclusions, three cases were analyzed: elastic and viscoelastic inclusions which are stiffer or softer than the matrix. Comparisons with Finite Element simulations have shown that accounting for particle-to-particle interactions enables to significantly improve accuracy of estimates (both in terms of overall and per phase responses) with respect to schemes ignoring these interaction effects (for instance the Mori-Tanaka model).

Moreover, the proposed interaction cluster model correctly predicts the overall anisotropy induced by the internal architecture of the composite (topology-induced anisotropy).

The model was shown to provide accurate results for the global response and for local fields up to relatively large volume fractions of inclusions (volume fraction of 0.25 in the worst case). Thus, at finite volume fractions of inclusions, taking account for inclusion-to-inclusion interactions is an essential aspect that cannot be achieved by classical homogenization schemes. To improve the quality of results for volume fractions of inclusion larger than 0.3, a strategy could be to enrich the present model by accounting for second order moments of local fields per phases.

All results were obtained under the framework of uniform strain boundary condition. It could be of interest to investigate the case of spatially slowly-varying strain field (quadratic displacement field) to capture the non-local effective response.

Altogether, the capacities of the proposed mean field interaction model to capture topological effects are opening interesting perspectives for architectured materials. In particular, the model could be used as an efficient tool for tuning the internal structure of composite materials to tailor desirable overall properties.

## Declaration of Competing Interest

The authors declare that they have no known competing financial interests or personal relationships that could have appeared to influence the work reported in this paper.

## Acknowledgement

The research was partially supported by the project No. 2016/23/B/ST8/03418 of the National Science Centre, Poland.

## Appendix A. Derivation of Eq. (20)

From Eq. (11) we have:

$$\left(\mathbf{P}^0\right)^{-1}\cdot(\boldsymbol{\epsilon}_0-\mathbf{E}) = f(\mathbf{C}_I\cdot\boldsymbol{\epsilon}_I-\mathbf{C}_m\cdot\boldsymbol{\epsilon}_I)+f\Delta\boldsymbol{\beta}_I\theta \tag{A.1}$$

Then, by using the strain average equation, $f\boldsymbol{\epsilon}_I = \mathbf{E}-(1-f)\boldsymbol{\epsilon}_m$, and the constitutive laws for inclusion and matrix phases, Eqs. (2,3), we obtain:

$$\left(\mathbf{P}^0\right)^{-1}\cdot(\boldsymbol{\epsilon}_0-\mathbf{E}) = f\boldsymbol{\sigma}_I+(1-f)\boldsymbol{\sigma}_m-\mathbf{C}_m\cdot\mathbf{E}-\boldsymbol{\beta}_m\theta \tag{A.2}$$

With the stress average equality and the definition of $\boldsymbol{\sigma}_0$, Eq. (14), to eliminate $\boldsymbol{\beta}_m\theta$ in Eq. (A.2), it follows that:

$$\left(\mathbf{P}^0\right)^{-1}\cdot(\boldsymbol{\epsilon}_0-\mathbf{E}) = \boldsymbol{\Sigma}-\boldsymbol{\sigma}_0+\mathbf{C}_m\cdot(\boldsymbol{\epsilon}_0-\mathbf{E}) \tag{A.3}$$

from which Eq. (20) results.

## Appendix B. System of first order differential equations governing the principal variables $\boldsymbol{\sigma}_I, \boldsymbol{\sigma}_m$ and $\boldsymbol{\sigma}_0$.

It is shown here that Eq. (68), Eq. (69) and Eq. (74) provide a linear system of first order differential equations governing the time evolution of the stresses $\boldsymbol{\sigma}_I, \boldsymbol{\sigma}_m$ and $\boldsymbol{\sigma}_0$.

Consider for instance Eq. (68). All terms are seen to be function of the principal variables $\boldsymbol{\sigma}_I, \boldsymbol{\sigma}_m, \boldsymbol{\sigma}_0$ and their time derivatives. This results from: (i) Eq. (70) for $\mathbf{d}_0$, (ii) Eq. (74) for $\mathbf{D}$, (iii) Eq. (54) for $\mathbf{M}_v^0(\mathbf{s}_m)$ and (iv) $\boldsymbol{\Sigma} = f\boldsymbol{\sigma}_I+(1-f)\boldsymbol{\sigma}_m$. Note that according to Eq. (70), $\mathbf{d}_0$ is linearly related to $\dot{\boldsymbol{\sigma}}_0$ and is depending upon $\boldsymbol{\sigma}_0$ and $\boldsymbol{\sigma}_m$ through $\mathbf{s}_0 = \mathrm{dev}(\boldsymbol{\sigma}_0)$ and $\mathbf{s}_m = \mathrm{dev}(\boldsymbol{\sigma}_\mathrm{m})$, since $\mathbf{M}_m^{\mathrm{tg}}$ and $\mathbf{d}_m^{\mathrm{ref}}$ are function of $\mathbf{s}_m$. Similarly, $\mathbf{d}_I$ and $\mathbf{d}_m$ are functions respectively of $\dot{\boldsymbol{\sigma}}_I, \boldsymbol{\sigma}_I$, and $\dot{\boldsymbol{\sigma}}_m, \boldsymbol{\sigma}_m$, through the constitutive law: $\mathbf{d}_k = \mathbf{M}_k\cdot\dot{\boldsymbol{\sigma}}_k+\mathbf{F}_k(\mathbf{s}_k)$, ($k = I$ for inclusion, $k = m$ for matrix). Thus, it appears

clearly that Eq. (68) is linearly dependent upon the stress rates $\dot{\boldsymbol{\sigma}}_I, \dot{\boldsymbol{\sigma}}_m$ and $\dot{\boldsymbol{\sigma}}_0$.

Similar considerations can be developed for Eq. (69) and Eq. (74).

## References


Abdul-Latif, A., Dingli, J., Saanouni, K., 1998. Modeling of complex cyclic inelasticity in heterogeneous polycrystalline microstructure. Mech. Mater. 30, 287–305. https://doi.org/10.1016/S0167-6636(98)00054-4.

Abdul-Latif, A., Miad, A.K.-E., Baleh, R., Garmestani, H., 2018. Modeling the mechanical behavior of heterogeneous ultrafine grained polycrystalline and nanocrystalline FCC metals. Mech. Mater. 126, 1–12. https://doi.org/10.1016/j.mechmat.2018.07.002.

Bacca, M., Bigoni, D., Dal Corso, F., Veber, D., 2013a. Mindlin second-gradient elastic properties from dilute two-phase Cauchy-elastic composites. Part I: Closed form expression for the effective higher-order constitutive tensor. Int. J. Solids Struct. 50, 4010–4019. https://doi.org/10.1016/j.ijsolstr.2013.08.014.

Bacca, M., Dal Corso, F., Veber, D., Bigoni, D., 2013b. Anisotropic effective higher-order response of heterogeneous Cauchy elastic materials. Mech. Res. Commun. 54, 63–71. https://doi.org/10.1016/j.mechrescom.2013.09.008.

Berveiller, M., Fassi-Fehri, O., Hihi, A., 1987. The problem of two plastic and heterogeneous inclusions in an anisotropic medium. Int. J. Eng. Sci. 25, 691–709. https://doi.org/10.1016/0020-7225(87)90058-9.

Bigoni, D., Drugan, W., 2007. Analytical derivation of Cosserat moduli via homogenization of heterogeneous elastic materials. ASME. J. Appl. Mech. 74, 741–753. https://doi.org/10.1115/1.2711225.

Bornert, M., Stolz, C., Zaoui, A., 1996. Morphologically representative pattern-based bounding in elasticity. J. Mech. Phys. Solids 44, 307–331. https://doi.org/10.1016/0022-5096(95)00083-6.

Czarnota, C., Kowalczyk-Gajewska, K., Salahouelhadj, A., Martiny, M., Mercier, S., 2015. Modeling of the cyclic behavior of elastic–viscoplastic composites by the additive tangent Mori-Tanaka approach and validation by finite element calculations. Int. J. Solids Struct. 56–57, 96–117. https://doi.org/10.1016/j.ijsolstr.2014.12.002.

Dal Corso, F., Deseri, L., 2013. Analytical derivation of Cosserat moduli via homogenization of heterogeneous elastic materials. Meccanica 48, 1901–1923..

Drugan, W., Willis, J., 1996. A micromechanics-based nonlocal constitutive equation and estimates of representative volume element size for elastic composites. J. Mech. Phys. Solids 44, 497–524. https://doi.org/10.1016/0022-5096(96)00007-5.

El Mouden, M., Cherkaoui, M., Molinari, A., Berveiller, M., 1998. The overall elastic response of materials containing coated inclusions in a periodic array. Int. J. Eng. Sci. 36, 813–829. https://doi.org/10.1016/S0020-7225(97)00111-0.

El Mouden, M., Molinari, A., 2000. Thermoelastic properties of composites containing ellipsoidal inhomogeneities. J. Therm. Stresses 23, 233–255. https://doi.org/10.1080/014957300280425.

Girard, G., Frydrych, K., Kowalczyk-Gajewska, K., Martiny, M., Mercier, S., 2021. Cyclic response of electrodeposited copper films. Experiments and elastic-viscoplastic mean-field modeling. Mech. Mater. 153,. https://doi.org/10.1016/j.mechmat.2020.103685 103685.

Hashin, Z., 1969. The inelastic inclusion problem. Int. J. Eng. Sci. 7, 11–36. https://doi.org/10.1016/0020-7225(69)90020-2.

Hatta, H., Taya, M., 1986. Thermal conductivity of coated filler composites. J. Appl. Phys. 59, 1851–1860. https://doi.org/10.1063/1.336412.

Hill, R., 1965. A self-consistent mechanics of composite materials. J. Mech. Phys. Solids 13, 213–222. https://doi.org/10.1016/0022-5096(65)90010-4.

Korelc, J., 2002. Multi-language and multi-environment generation of nonlinear finite element codes. Eng. Comput. 18, 312–327. https://doi.org/10.1007/s003660200028.

Kouddane, R., Molinari, A., Canova, G.R., 1993. Proceedings of the international seminar MECAMAT 91, Fontainebleau/France/7-8 august 1991. chapter Self-consistent modelling of heterogeneous viscoelastic and elastoviscoplastic materials. (pp. 129–141). A.A.Balkema.

Kowalczyk-Gajewska, K., Petryk, H., 2011. Sequential linearization method for viscous/elastic heterogeneous materials. Eur. J. Mech. Solids/A 30, 650–664. https://doi.org/10.1016/j.euromechsol.2011.04.002.

Kushch, V.I., Mogilevskaya, S.G., Stolarski, H.K., Crouch, S.L., 2013. Evaluation of the effective elastic moduli of particulate composites based on Maxwell's concept of equivalent inhomogeneity: microstructure-induced anisotropy. J. Mech. Mater. Struct. 8, 283–303. https://doi.org/10.2140/jomms.2013.8.283.

Lahellec, N., Suquet, P., 2007. On the effective behavior of nonlinear inelastic composites: I. Incremental variational principles. J. Mech. Phys. Solids 55, 1932–1963. https://doi.org/10.1016/j.jmps.2007.02.003.

Li, D., Hu, G.-K., 2007. Effective viscoelastic behavior of particulate polymer composites at finite concentration. Appl. Math. Mech.-Engl. Ed. 28, 297–307. https://doi.org/10.1007/s 10483-007-0303-1.

Lu, S., 1999. Effective conductivities of rectangular array of aligned spheroids. J. Appl. Phys. 85, 264–269. https://doi.org/10.1063/1.369439.

Lu, S., Song, J., 1996. Effective conductivity of composites with spherical inclusions: Effect of coating and detachment. J. Appl. Phys. 79, 609–618. https://doi.org/10.1063/1.360803.

Ma, H., Hu, G., Huang, Z., 2004. A micromechanical method for particulate composites with finite particle concentration. Mech. Mater. 36, 359–368. https://doi.org/10.1016/S0167-6636(03)00065-6.

Majewski, M., Holobut, P., Kursa, M., Kowalczyk-Gajewska, K., 2020. Packing and size effects in elastic-plastic particulate composites: Micromechanical modelling and numerical verification. Int. J. Eng. Sci. 151,. https://doi.org/10.1016/j.ijengsci.2020.103271 103271.

Majewski, M., Kursa, M., Holobut, P., Kowalczyk-Gajewska, K., 2017. Micromechanical and numerical analysis of packing and size effects in elastic particulate composites. Compos. B 124, 158–174. https://doi.org/10.1016/j.compositesb.2017.05.004.

Marcadon, V., Herve, E., Zaoui, A., 2007. Micromechanical modeling of packing and size effects in particulate composites. Int. J. Solids Struct. 44, 8213–8228. https://doi.org/10.1016/j.ijsolstr.2007.06.008.

McKenzie, D., McPhedran, R., Derrick, G.H., 1978. The conductivity of lattice of spheres II. The body centred and face centred cubic lattices. Proc. R. Soc. Lond. 362, 211–232. https://doi.org/10.1098/rspa.1978.0129.

McPhedran, R., McKenzie, D., 1978. The conductivity of lattice of spheres I. The simple cubic lattice. Proc. R. Soc. Lond. 359, 45–63. https://doi.org/10.1098/rspa.1978.0031.

Mercier, S., Jacques, N., Molinari, A., 2005. Validation of an interaction law for the Eshelby inclusion problem in elasto-viscoplasticity. Int. J. Solids and Struct. 42, 1923–1941. https://doi.org/10.1016/j.ijsolstr.2004.08.016.

Mercier, S., Kowalczyk-Gajewska, K., Czarnota, C., 2019. Effective behavior of composites with combined kinematic and isotropic hardening based on additive tangent Mori-Tanaka scheme. Compos. Part B: Eng. 174,. https://doi.org/10.1016/j.compositesb.2019.107052 107052.

Mercier, S., Molinari, A., 2009. Homogenization of elastic-viscoplastic heterogeneous materials: Self-consistent and Mori-Tanaka schemes. Int. J. Plast. 25, 1024–1048. https://doi.org/10.1016/j.ijplas.2008.08.006.

Mercier, S., Molinari, A., Berbenni, S., Berveiller, M., 2012. Comparison of different homogenization approaches for elastic-viscoplastic materials. Model. Simul. Mater. Sci. Eng. 20,. https://doi.org/10.1088/0965-0393/20/2/024004 024044.

Mercier, S., Molinari, A., El Mouden, M., 2000. Thermal conductivity of composite material with coated inclusions: Applications to tetragonal array of spheroids. J. Appl. Phys. 87, 3511. https://doi.org/10.1063/1.372374.

Molinari, A., 2002. Averaging models for heterogeneous viscoplastic and elastic viscoplastic materials. J. Eng. Mater. Technol. Trans. ASME 124, 62–70. https://doi.org/10.1115/1.1421052.

Molinari, A., Ahzi, S., Kouddane, R., 1997. On the self-consistent modeling of elastic-plastic behavior of polycrystals. Mech. Mater. 26, 43–62. https://doi.org/10.1016/S0167-6636(97)00017-3.

Molinari, A., Canova, G.R., Ahzi, S., 1987. Self-consistent approach of the large deformation polycrystal visco-plasticity. Acta Metall. 35, 2983–2994. https://doi.org/10.1016/0001-6160(87)90297-5.

Molinari, A., El Mouden, M., 1996. The problem of elastic inclusions at finite concentration. Int. J. Solids Struct. 33, 3131–3150. https://doi.org/10.1016/0020-7683(95)00275-8.

Monetto, I., Drugan, W., 2009. A micromechanics-based nonlocal constitutive equation and minimum RVE size estimates for random elastic composites containing aligned spheroidal heterogeneities. J. Mech. Phys. Solids 57, 1578–1595. https://doi.org/10.1016/j.jmps.2009.05.005.

Nemat-Nasser, S., Iwakuma, T., Hejazi, M., 1982. On composites with periodic structure. Mech. Mater. 1, 239–267. https://doi.org/10.1016/0167-6636(82)90017-5.

Ponte Castañeda, P., Willis, J., 1995. The effect of spatial distribution on the effective behavior of composite materials and cracked media. J. Mech. Phys. Solids 43, 1919–1951. https://doi.org/10.1016/0022-5096(95)00058-Q.

Rayleigh, L., 1892. On the influence of obstacles arranged in rectangular order upon the properties of a medium. Philos. Mag. 34, 481–502. https://doi.org/10.1080/14786449208620364.

Rodin, G.J., 1993. The overall elastic response of materials containing spherical inhomogeneities. Int. J. Solids Struct. 30, 1849–1863. https://doi.org/10.1016/0020-7683(93)90221-R.

Sangani, A., Acrivos, A., 1982. The effective conductivity of a periodic array of spheres. Proc. R. Soc. Lond. 386, 263–275. https://doi.org/10.1098/rspa.1983.0036.

Sangani, A.S., Lu, W., 1987. Elastic coefficients of composites containing spherical inclusions in a periodic array. J. Mech. Phys. Solids 35, 1–21. https://doi.org/10.1016/0022-5096(87)90024-X.

Schjødt-Thomsen, J., Pyrz, R., 2005. Cubic inclusion arrangement: effect on stress and effective properties. Comput. Mater. Sci. 34, 129–139. https://doi.org/10.1016/j.commatsci.2004.12.061.

Wang, H., Wu, P.D., Tomé, C.N., Huang, Y., 2010. A finite strain elastic-viscoplastic self-consistent model for polycrystalline materials. J. Mech. Phys. Solids 58, 594–612. https://doi.org/10.1016/j.jmps.2010.01.004.

Zecevic, M., Lebensohn, R.A., 2020. New robust self-consistent homogenization schemes of elasto-viscoplastic polycrystals. Int. J. Solids Struct. 202, 434–453. https://doi.org/10.1016/j.ijsolstr.2020.05.032.

Zeller, R., Dederichs, P., 1973. Elastic constant of polycrystals. Phys. Status Solidi B 55, 831–842. https://doi.org/10.1002/pssb.2220550241.